Distribution of a Glycosylphosphatidylinositol-anchored Protein at the Apical Surface of MDCK Cells Examined at a Resolution of <100 Å Using Imaging Fluorescence Resonance Energy Transfer

A.K. Kenworthy and M. Edidin

Department of Biology, Johns Hopkins University, Baltimore, Maryland 21218

Abstract. Membrane microdomains ("lipid rafts") enriched in glycosylphosphatidylinositol (GPI)-anchored proteins, glycosphingolipids, and cholesterol have been implicated in events ranging from membrane trafficking to signal transduction. Although there is biochemical evidence for such membrane microdomains, they have not been visualized by light or electron microscopy. To probe for microdomains enriched in GPI-anchored proteins in intact cell membranes, we used a novel form of digital microscopy, imaging fluorescence resonance energy transfer (FRET), which extends the resolution of fluorescence microscopy to the molecular level (<100 Å). We detected significant energy transfer between donor- and acceptor-labeled antibodies against the GPI-anchored protein 5′ nucleotidase (5′ NT) at the apical membrane of MDCK cells. The efficiency of energy transfer correlated strongly with the surface density of the acceptor-labeled antibody. The FRET data conformed to theoretical predictions for two-dimensional FRET between randomly distributed molecules and were inconsistent with a model in which 5′ NT is constitutively clustered. Though we cannot completely exclude the possibility that some 5′ NT is in clusters, the data imply that most 5′ NT molecules are randomly distributed across the apical surface of MDCK cells. These findings constrain current models for lipid rafts and the membrane organization of GPI-anchored proteins.

Key words: cell membrane • cell polarity • 5′ nucleotidase• fluorescence microscopy • membrane lipids

GLYCOSYLPHOSPHATIDYLINOSITOL (GPI)[1]-anchored proteins are attached to the membrane bilayer by a complex anchor consisting of phosphoethanolamine, glycans, and phosphatidylinositol lipid (Low, 1989). In biological membranes, GPI-anchored proteins are thought to reside in membrane microdomains (also know as "rafts" or detergent-insoluble, glycolipid-enriched complexes) that are enriched in glycosphingolipids (GSL) and cholesterol (for reviews see Simons and van Meer, 1988; Lisanti and Rodriguez-Boulan, 1990; Simons and Wandinger-Ness, 1990; Harder and Simons, 1997; Simons and Ikonen, 1997). It has been suggested that these microdomains are important for the apical sorting of GPI-anchored proteins in polarized cells (Brown et al., 1989; Lisanti et al., 1989; Lisanti and Rodriguez-Boulan, 1990) and for intracellular signaling after cross-linking of GPI-anchored and transmembrane proteins (Lisanti et al., 1994; Field et al., 1997; Harder and Simons, 1997; Simons and Ikonen, 1997).

Evidence for membrane microdomains comes from biochemical experiments in which the differential solubility of membrane proteins and lipids in detergent is used as the criterion for defining a microdomain (Stefanova et al., 1991; Brown and Rose, 1992; Sargiacomo et al., 1993; Arreaza et al., 1994). However, other studies indicate that proteins and lipids sharing the common property of detergent insolubility are not necessarily associated in intact cell membranes (Kurzchalia et al., 1995; Mayor and Maxfield, 1995; Schnitzer et al., 1995, 1996; Hannan and Edidin, 1996). Furthermore, electron and fluorescence microscopy of intact cells usually do not detect membrane

Address all correspondence to A.K. Kenworthy, Department of Biology, Johns Hopkins University, 3400 N. Charles St., Baltimore, MD 21218. Tel.: (410) 516-7295. Fax: (410) 516-5213. E-mail: kenwrthy@jhuvms.hcf.jhu.edu

1. *Abbreviations used in this paper*: 5′ NT, 5′ nucleotidase; c_A, reduced acceptor surface density; c_D, reduced donor surface density; D:A, molar donor/acceptor ratio; E, energy transfer efficiency; $E_{clustered}$, theoretical energy transfer efficiency for clustered molecules; $E_{mixture}$, theoretical energy transfer efficiency for a mixture of randomly distributed and clustered molecules; E_{random}, theoretical energy transfer efficiency for randomly distributed molecules; f_A, mole fraction of acceptors; f_D, mole fraction of donors; f_U, mole fraction of unlabeled molecules; $f_{clustered}$, fraction of clustered molecules; f_{random}, fraction of randomly distributed molecules; Fab, monovalent antibody fragment; FRET, fluorescence resonance energy transfer; GPI, glycosylphosphatidylinositol; GSL, glycosphingolipids.

microdomains enriched in GPI-anchored proteins. Early work that visualized clusters of GPI-anchored proteins used secondary antibodies (Rothberg et al., 1990), which themselves may have induced cross-linking (Mayor et al., 1994; Fujimoto, 1996). Studies also indicate that at steady state, in the absence of cross-linking, GPI-anchored proteins are randomly distributed in the plasma membrane (Parton et al., 1994; Rijnboutt et al., 1996). This result is consistent with work from our laboratory using a biophysical method, fluorescence resonance energy transfer (FRET) microscopy. Though FRET can detect the close proximity of molecules, we found no evidence for FRET between labeled GPI-anchored proteins under steady-state conditions (Hannan et al., 1993). Recently, Harder and Simons (1997) attempted to resolve these disparate results by suggesting that the insoluble domains isolated by detergent extraction represent coalesced microdomains of unknown size, morphology, and composition. In this view, microscopy-based techniques fail to detect microdomains in intact cell membranes because the domains are small, dynamic structures that are below the resolution limit of the microscope.

The continued discrepancy between the apparent enrichment of GPI-anchored proteins in membrane microdomains reported by biochemical methods and the random steady-state distribution of these proteins reported by microscopy have led us to use a new method, imaging FRET, to critically reexamine the steady-state membrane organization of a GPI-anchored protein. Imaging FRET combines digital immunofluorescence microscopy with FRET, a phenomenon that reports proximity between molecules on a length scale of 1–10 nm. Imaging FRET thus increases the resolution of conventional immunofluorescence microscopy to the molecular level and so allows one to quantitatively assess molecular proximity in intact cell membranes (Herman, 1989; Jovin and Arndt-Jovin, 1989*a*,*b*; Tsien et al., 1993; Uster, 1993; Selvin, 1995). Imaging FRET maps energy transfer between molecules of interest on a cell-by-cell basis, a substantial advance over our previous microscopic FRET method, which measured the average FRET for a cell population (Hannan et al., 1993). By comparing experimental FRET values with theoretical predictions for randomly distributed molecules, imaging FRET measurements can be used to infer the organization of molecules—clustered or randomly distributed—in cell membranes. Hence, imaging FRET should be able to detect enrichment of GPI-anchored proteins in membrane microdomains too small to be resolved by light microscopy, as long as GPI-anchored proteins in the domain are within <100 Å of one another.

In this study, we evaluate the steady-state distribution of a GPI-anchored protein, 5′ nucleotidase (5′ NT), in the apical plasma membrane of transfected MDCK cells. Detergent-insoluble complexes containing GPI-anchored proteins and GSL were first identified in MDCK cells (Brown and Rose, 1992), and this cell line has been used extensively in studies of protein sorting (Simons and Ikonen, 1997). 5′ NT (CD73) is a 70-kD ectoenzyme that catalyzes the hydrolysis of 5′ AMP to adenosine (for review see Zimmermann, 1992). 5′ NT is enriched in detergent-insoluble complexes in several different cell systems (Mescher et al., 1981; Schnitzer et al., 1995; Strohmeier et al., 1997), is sometimes found in clusters by immunoelectron microscopy (Howell et al., 1987), and upon antibody cross-linking can trigger intracellular signaling events in some cell types (Airas et al., 1997; Resta and Thompson, 1997).

To see if 5′ NT is distributed randomly on the apical membrane of MDCK cells, or if it is enriched in membrane microdomains, we combined imaging FRET with the theory previously developed for two-dimensional FRET. FRET between labeled 5′ NT molecules should be detectable whether or not they are clustered in membrane microdomains, since FRET may also occur between randomly distributed molecules present at high surface density. However, the theory for FRET between donors and acceptors in a membrane allows us to distinguish between clustered 5′ NT molecules, randomly distributed 5′ NT molecules, and mixtures of the two. As expected, we detected FRET under steady-state conditions. The relationships between the extent of FRET, surface concentration of 5′ NT, and proportions of donor and acceptor labels indicate that the majority, if not all 5′ NT molecules are randomly distributed and are not clustered or confined to lipid rafts.

Materials and Methods

Cells

The full-length 5′ NT cDNA from rat liver (clone pcNT341) was the generous gift of Dr. Y. Ikehara (Misumi et al., 1990). pcNT341 was inserted into EcoRI site of pCB6 (Brewer, 1994) modified to contain a portion of the Bluescript multicloning site. MDCK cells (type II) were transfected using a calcium phosphate precipitation method (Weisz et al., 1992) and selected in medium containing 500 μg/ml G418 (GIBCO BRL, Gaithersburg, MD). Positive clones were isolated using cloning rings and screened by indirect immunofluorescence microscopy. One of the positive clones was then subcloned by cell sorting, followed by seeding at limiting dilution with untransfected cells.

After cloning, cells were maintained in DME (GIBCO BRL, Gaithersburg, MD) supplemented with 10% fetal calf serum (INTERGEN Co., Purchase, NY), nonessential amino acids (GIBCO BRL), and 300 μg/ml G418. Propagation stocks were passaged at a 1:50 dilution every 4–6 d. Cells for experiments were plated onto sterile coverslips at a 1:5 dilution ($\sim 1 \times 10^6$ cells/10-cm plate, six coverslips/plate, transferred to six-well dishes the following day) and grown to confluence (2–5 d). For the biotinylation experiments, cells were plated onto filters (Falcon HD Cell Culture Inserts, six-well format, 0.4-μm pore size; Becton Dickinson Labware, Franklin Lakes, NJ) at a density of $\sim 1 \times 10^6$ cells. Where indicated, 5′ NT expression was enhanced by overnight incubation in medium containing 10 mM sodium butyrate before an experiment.

Antibodies

A hybridoma producing the mouse monoclonal IgG antibody 5NT4-2 (Siddle et al., 1981) was the generous gift of Dr. P. Luzio. This antibody inhibits 5′ NT enzyme activity by a maximum of ~50% (Siddle et al., 1981). Thus, although 5′ NT is thought to form a dimer (Zimmermann, 1992) we expect this antibody to bind only one monomer per dimer. 5NT4-2 IgG was purified from ascites using E-Z-Sep (Pharmacia Biotech Inc., Piscataway, NJ) or from hybridoma supernatant using a protein A–Sepharose column. Monovalent antibody fragments (Fab) were prepared from IgG using published methods (Matko and Edidin, 1997). The final Fab fraction was incubated with protein A–Sepharose to remove any remaining IgG. Bisfunctional succinimidyl ester derivatives of the cyanine dyes Cy3 and Cy5 (Southwick et al., 1990; Mujumdar et al., 1993) were conjugated to purified Fab and IgG as per the manufacturer's instructions (Fluorolink Reactive Dye; Amersham Life Science, Inc., Arlington Heights, IL). The conjugation reaction was stopped by passing it over a column (10DG column; BioRad Laboratories, Hercules, CA) to separate the conjugated proteins from the unbound dye. The final dye/protein val-

ues were 2.9 and 1.7 for the Cy3 and Cy5 IgG conjugates, and 6.3 and 4.1 for the Cy3 and Cy5 Fab conjugates, respectively.

5′ NT Release with Phosphatidylinositol-specific Phospholipase C

The GPI-anchorage of 5′ NT in the transfected MDCK clones was confirmed by phospholipase C treatment of Triton X-114 cell extracts (Hannan and Edidin, 1996) using precondensed Triton X-114 (Bordier, 1981). 5′ NT was immunoprecipitated from Triton X-114 enriched and depleted phases, subjected to SDS-PAGE, transferred to a Western blot, and detected by enhanced chemiluminescence (ECL; Amersham Life Science, Inc.).

Polarity of 5′ NT Surface Expression

Surface-specific biotinylation (Weisz et al., 1992) was performed on cells grown on filters. 5′ NT expression was enhanced by overnight incubation in medium containing 10 mM sodium butyrate. Before the experiment, the tightness of the monolayers was tested by assaying for leakage to the basolateral compartment of [^{3}H]inulin added to the apical compartment. Immunoprecipitated, biotinylated 5′ NT was subjected to SDS-PAGE, transferred to a Western blot, and detected by enhanced chemiluminescence. The blots were quantified by densitometry. Polarity of surface biotinylated 5′ NT expression was determined as apical/(apical + basolateral).

Immunofluorescence Labeling

Cells on coverslips were labeled for 15 min at 4°C with 100 μl of a mixture of donor (Cy3)- and acceptor (Cy5)-labeled antibodies. In all experiments, the antibodies were diluted in PBS supplemented with 0.9 mM $CaCl_2$, 0.52 mM $MgCl_2$, and 0.16 mM $MgSO_4$ (PBS^{++}) containing 1% BSA. The cells were rinsed twice for 5 min in PBS^{++} at 4°C. The cells were then fixed for 30 min at room temperature in 4% formaldehyde in PBS^{++}, freshly prepared from a 16% formaldehyde solution (Electron Microscopy Sciences, Ft. Washington, PA). Finally, the coverslips were mounted on slides in PBS, with 50-μm-thick pieces of tape used to hold the coverslips away from the slide, and then sealed with nail polish. Note that we chose to fix the cells before the microscopy measurements to prevent potential reorganization of the proteins during the course of the experiments. To this point, in experiments where the cells were labeled with fluorophore-conjugated primary antibodies (IgG) and then shifted to 37°C for 30 min, the label appeared more "patchy" than in controls that had been immediately fixed.

Unless otherwise indicated, the concentration of Cy3-conjugated antibody was held constant at 50 μg/ml in each mixture, and Cy5-conjugated antibody was added to give the indicated molar ratio of donor to acceptor (D:A). In a control experiments, the saturating antibody concentration was determined to be ~200 μg/ml. Thus in the FRET experiments, the total antibody concentration ranged from subsaturating to saturating. The experimentally measured ratio of donor to acceptor fluorescence was directly proportional to D:A applied to the cells.

In experiments measuring FRET between primary and secondary antibodies, cells were labeled with 50 μg/ml of Cy3-5NT4-2 IgG as above, washed twice in PBS^{++} for 5 min at 4°C, incubated for 15 min at 4°C with either 5 or 50 μg/ml of Cy5-labeled secondary antibody (donkey anti–mouse H + L, dye/protein ratio ~1.6; Jackson ImmunoResearch Laboratories, West Grove, PA), washed again, and then immediately fixed. The amount of Cy5 secondary antibody that bound increased only about twofold based on its relative fluorescence intensity, despite the 10-fold difference in concentration.

When secondary antibody was used to cross-link labeled 5′ NT, cells were labeled with the indicated D:A of 5NT4-2 IgG as above and then washed twice with PBS^{++} for 5 min at 4°C. The cells were then incubated for 15 min at 4°C in the presence or absence of 10 μg/ml unlabeled secondary antibody (donkey anti–mouse H + L; Jackson ImmunoResearch Laboratories). After washing as before, the cells labeled without secondary antibody were fixed immediately. The cells labeled in the presence of secondary antibody were either fixed immediately or were incubated at 37°C for 15 min before fixation.

In the detergent extraction experiments, cells were labeled for 15 min at 4°C with 1:1 D:A of 5NT4-2 IgG, followed by a 30-min incubation at 4°C in either PBS^{++} or PBS^{++} containing 1% Triton X-100. The cells were then rinsed briefly with cold PBS^{++} and fixed in 4% formaldehyde as above.

Imaging

Cells were imaged on a fluorescence microscope (model Axiovert 135TV; Carl Zeiss, Inc., Thornwood, NY) using a 1.4 NA 63× Zeiss Plan-apochromat objective or a 1.3 NA 100× Zeiss Plan-neofluor objective. Digital images were collected using the IC300 digital imaging system (Inovision, Research Triangle Park, NC). Cy3 and Cy5 were detected using appropriate filter sets (Cy3 filter cube: excitation 515–560 nm, 565-nm long pass dichroic, emission 573–648 nm; Cy5 filter cube: excitation 590–650 nm, 660-nm long pass dichroic, emission 663–738 nm) (Chroma Technology Corporation, Brattleboro, VT). Images were collected with a Series 200 cooled CCD camera with a 1,340 × 1,037-pixel ICAF-1400 chip (Photometrics, Tucson, AZ). Fluorescence was excited with a 75-W xenon arc lamp. Image acquisition time was adjusted to maximize the range of CCD. Using typical exposure times for image acquisition (less than 5 s), no fluorescence was observed from a Cy3-labeled specimen using the Cy5 filters, nor was Cy5 fluorescence detected using the Cy3 filter sets.

Imaging FRET Measurements

FRET is widely used as a spectroscopic tool for detecting molecular interactions and molecular proximity in solution, as well as in membranes. It involves the nonradiative transfer of energy from the excited state of a donor molecule to an appropriate acceptor (Wu and Brand, 1994; Clegg, 1995, 1996).

The rate of energy transfer is inversely proportional to the sixth power of the distance, r, between the donor and acceptor. The efficiency of energy transfer E is defined with respect to r and R_o, the characteristic Förster distance for the donor and acceptor pair by

$$E = 1/[1 + (r/R_o)^6]. \quad (1)$$

For example, when $r = R_o$, E is 50%, and when $r = 2R_o$, E is 1.5%. The value of R_o depends on the relative orientation of the donor and acceptor, the overlap interval between the emission spectrum of the donor and the excitation spectrum of the acceptor, and the fluorescence quantum yield of the donor. In our experiments, Cy3 was used as a donor, and Cy5 as an acceptor. R_o for this donor and acceptor pair has been calculated as 50 Å (Bastiaens and Jovin, 1996), assuming an orientation factor, κ^2, of 2/3 (Dale et al., 1979). For this value of R_o, when r = 50 Å, E is 50%, and when r = 100 Å, E is 1.5%.

Experimentally, FRET can be detected in several ways. Energy transfer causes quenching of donor fluorescence and sensitized fluorescence of the acceptor. It also reduces the donor lifetime and decreases the rate of irreversible photobleaching of the donor (Clegg, 1995, 1996). Imaging FRET techniques have been developed to measure all of these events. Methods described to date to measure energy transfer follow donor photobleaching (Kubitscheck et al., 1991, 1993; Hannan et al., 1993; Damjanovich et al., 1995; Gadella and Jovin, 1995; Jurgens et al., 1996), variations on sensitized acceptor fluorescence (Uster and Pagano, 1986; Adams et al., 1991; Bacskai et al., 1993; Kam et al., 1995), donor quenching (Kindzelskii et al., 1994; Xue et al., 1994; Bastiaens and Jovin, 1996; Bastiaens et al., 1996; Kindzelskii et al., 1996), and donor lifetimes (Oida et al., 1993).

In the present study, FRET was measured using a method developed for a laser confocal microscope (Bastiaens and Jovin, 1996; Bastiaens et al., 1996) modified by us for use with a conventional arc lamp microscope (Kenworthy and Edidin, 1997). In this method, samples are labeled with a mixture of donor- and acceptor-conjugated antibodies, and energy transfer is detected as an increase in donor fluorescence (dequenching) after complete photobleaching of the acceptor fluorophore. An advantage of this method is that all the parameters needed to quantitate E can be obtained from the same field of cells, eliminating the need to correct for differences in the amount of donor antibody bound in samples separately labeled with donor and acceptor (or only with donor) or to determine spectral correction factors necessary to quantitate sensitized acceptor fluorescence measurements (Jovin and Arndt-Jovin, 1989*a*,*b*). The validity of using donor dequenching to quantify FRET depends on the fact that the only factor that can lead to a difference in donor fluorescence in the presence and absence of acceptor is energy transfer.

To quantitatively measure E with this method, the acceptor must be sufficiently photolabile that it can be completely bleached, and the donor fluorescence must not fade significantly while images are acquired in the presence and absence of the acceptor. Cells labeled with Cy5-conjugated IgG were used to determine the minimum time required to completely bleach the Cy5. Typically, Cy5 was completely photobleached by 7 min or less of continuous arc lamp excitation using a Cy5 filter set and an addi-

tional 570-nm long pass filter in the excitation path. Under these conditions, greater than 97% of the Cy5 was bleached, and no Cy3 was bleached in control samples labeled with Cy3 IgG only. (In the absence of the long pass filter, a small amount of Cy3 was bleached during Cy5 bleaching.) This shows that Cy3 is stable enough to allow quantitative comparisons of donor fluorescence before and after acceptor photobleaching. Note that in these experiments, the Cy5 was bleached from an entire field of cells.

To perform an imaging FRET experiment, samples were labeled with both Cy3- and Cy5-conjugated antibodies in the indicated molar ratios, as described above. An initial image of Cy3 fluorescence (in the presence of the Cy5-conjugated antibodies) was obtained using Cy3 filter set. An image of Cy5 fluorescence was obtained using the Cy5 filter set and an additional 570-nm long pass filter in the excitation path, and then the sample was continuously illuminated for 7 min. An image of Cy5 fluorescence after photobleaching (<3% of the initial intensity) was then obtained, the long pass filter was removed, and another Cy3 fluorescence image was collected using the Cy3 filter set. Data were collected for four to five different fields from a single coverslip. The fluorescence intensities are reported in arbitrary units and are comparable within a given experiment, but they cannot be compared directly between experiments.

Images mapping FRET between labeled 5′ NT molecules were calculated from the increase in donor fluorescence after acceptor photodestruction by

$$E(\%) \times 100 = 10{,}000 \times [(\text{Cy3 postbleach} - \text{Cy3 prebleach}) / \text{Cy3 postbleach}] \quad (2)$$

after subtracting the dark current contribution and correcting the registration of the images using the Isee Pratt Index registration algorithm. The scaling factor of 10,000 was used to expand E (which scales from 0–1) to the scale of the 12-bit images (0–4,096). A value of 4,096 thus corresponds to E of 0.4096, or 40.96%. For cells labeled with donor only (D:A = 1:0), no significant energy transfer was observed (E < 2–3%).

The energy transfer efficiency images can potentially be analyzed on a pixel-by-pixel basis. However, because cell-to-cell variations in E contain information about the distribution of 5′ NT (see below), for further analysis we averaged over 40 × 40-pixel regions of interest (17.64 μm^2 at 63×, or 6.97 μm^2 at 100×) chosen from cells that were in focus. One region of interest was chosen per cell, and these areas were chosen so that they avoided the edges of the cells, where artifacts in the energy transfer efficiency images sometimes occurred. The mean fluorescence intensities and E were calculated for identical regions of interest for the registered Cy3 prebleach, Cy5 prebleach, Cy3 postbleach, and E images. Between 10 and 30 regions of interest were chosen from each field of cells, such that cells covering the complete range of 5′ NT expression levels were sampled. In experiments where clustering of 5′ NT was induced by secondary antibody, data were also collected with 5 × 5-pixel square regions of interest for areas on cells that were either depleted of 5′ NT or enriched in clusters. Because of the small sampling size, these data were more noisy and were scattered around the average E obtained using 40 × 40-pixel sample areas (data not shown).

Fluorescent Calibration Standards

Beads binding known numbers of IgGs ("Quantum Simply Cellular Beads," Flow Cytometry Standards Corporation, San Juan, Puerto Rico) were labeled with saturating concentrations of the same antibodies used to label the cells at room temperature for 1 h, washed twice in PBS, and then mounted under a coverslip in PBS. The saturating antibody concentration was titrated for Cy3-conjugated antibody by flow cytometry, and the same concentration was then used to label the Cy5 beads. The fluorescence intensity of beads was measured by collecting images while focusing at the maximum apparent diameter of the bead or above and then summing the intensity within a circular region of interest that just included the entire bead. (Control experiments established that the integrated fluorescence intensity associated with a bead was essentially constant for focal planes ranging from the top to the center [maximum apparent diameter] of the bead.) We then generated a calibration curve of total fluorescence intensity for a given number of acceptor-labeled antibodies. Using this, we calculated the number of acceptor-bound antibodies on the cells. Several assumptions were made to perform this calculation. First, we assumed that one monoclonal antibody binds one protein on the cell surface. Second, it was assumed that all the fluorophores bound to the bead contributed to the observed fluorescence intensity. This could underestimate the average fluorescence per fluorophore if the beads are not completely transparent. Third, the surface area of the apical plasma membrane was assumed to correspond to its projected area in the image. This would tend to underestimate this area because it ignores surface details such as microvilli.

Results

GPI-anchored 5′ NT Is Expressed on the Apical Membrane of MDCK Cells

5′ NT was expressed predominantly on the apical membrane of transfected MDCK cells. When living cells expressing 5′ NT were labeled with a fluorophore-conjugated monoclonal antibody and then fixed before imaging, fluorescence was distributed uniformly across most of the apical membrane and concentrated in punctate structures, likely microvilli (see Fig. 1). In cells grown on filters, fixed, and labeled from the basolateral surface, a small amount of basolateral fluorescence was apparent (data not shown). The polarity of 5′ NT surface expression was 73.3 ± 0.1% (n = 3) apical based on domain-specific biotinylation of cells in which 5′ NT expression was induced before the experiment. This predominantly but not exclusively apical polarization is similar to the polarity of 5′ NT in human intestinal epithelial cells (Strohmeier et al., 1997). The cell-to-cell variation in the expression of 5′ NT is typical of transfected MDCK cells (Lisanti et al., 1989). That 5′ NT was GPI-anchored in the transfected cells was confirmed in cell extracts, where 5′ NT shifted from a Triton X-114 detergent–enriched phase to an aqueous phase after phosphatidylinositol-specific phospholipase C treatment (data not shown).

FRET as a Measure of Molecular Clustering

In experiments that follow, we use FRET to determine the membrane distribution of the GPI-anchored protein 5′ NT. We do this by testing properties of the observed FRET against predictions for FRET based on the theory in the Appendix, summarized in Table I. First, we measure the dependence of energy transfer on donor and acceptor

Table I. Summary of the Theoretical Predictions for FRET for Various Distributions of Donor- and Acceptor-labeled Molecules in Membranes

Test	Predictions for		
	Randomly distributed molecules*	Mixture of clustered and randomly distributed molecules‡	Clustered molecules§
1. E is dependent on acceptor surface density	yes	yes	no
2. E is dependent on donor surface density	no‖	no	no
3. E goes to zero at low surface densities	yes	sometimes	no
4. E is sensitive to the donor: acceptor ratio	no¶	yes	yes

See Appendix for a detailed discussion of each case, including any additional assumptions or limitations.
*Derived from Eqs. A1 and A2 and illustrated in Fig. A2.
‡Derived from Eq. A5 and illustrated in Fig. A3.
§Derived from Eq. A4.
‖In the limit where excited state donors do not compete for acceptors.
¶So long as the acceptor concentration is kept constant.

surface density and D:A for cells expressing a wide range of 5′ NT surface densities, using both monovalent and bivalent antibodies as probes. Second, we estimate the absolute surface density of acceptor-labeled 5′ NT so that we can directly compare our data to theoretical curves. Finally, we measure energy transfer for molecules known to "cluster," primary and secondary antibodies, and for two different conditions previously shown to induce clustering of GPI-anchored proteins, cross-linking with secondary antibodies, and detergent extraction.

Energy Transfer Is Detected between Labeled 5′ NT Molecules, and It Correlates with the Surface Density of 5′ NT

We measured FRET in terms of dequenching of donor fluorescence after complete photobleaching of the acceptor fluorophore. Data from a typical imaging FRET experiment are shown in Fig. 1. The initial donor (Cy3) image represents donor fluorescence in the presence of acceptor, Cy5 (Fig. 1 *a*). As expected, the Cy5 image collected before photobleaching (Fig. 1 *b*) was identical to the Cy3 image since the same antibody was used for both the donor and acceptor label. After completely bleaching acceptor (Cy5) (Fig. 1 *d*), a second donor (Cy3) image was collected (Fig. 1 *c*). The fluorescence of the donor (Cy3) in some of the cells increased (Fig. 1, *a* and *c*, *arrows*), while in other cells, there was little to no change in donor fluorescence (Fig. 1, *a* and *c*, *arrowheads*). Increased donor fluorescence after destruction of the acceptor indicated that donor fluorescence was quenched in the presence of the acceptor because of energy transfer. In general, the largest dequenching was observed in cells expressing the highest amounts of protein.

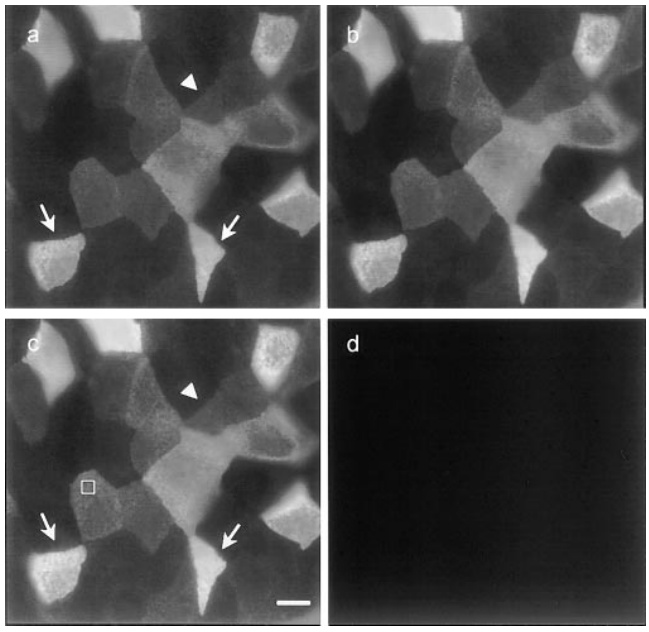

Figure 1. Energy transfer can be detected from the increase in donor fluorescence after acceptor photobleaching. (*a*) Donor (Cy3) image before acceptor photobleaching, (*b*) acceptor (Cy5) image before photobleaching, (*c*) donor (Cy3) image after acceptor (Cy5) photobleaching, and (*d*) acceptor (Cy5) image after photobleaching. In this experiment, the cells were labeled with donor- and acceptor-conjugated IgG at D:A of 1:3. Bar, 10 μm.

Images of *E* were calculated from the donor images obtained before and after acceptor photodestruction, using Eq. 2. The calculated *E* image for the data of Fig. 1 is shown in Fig. 2 *a*. There was significant energy transfer between labeled 5′ NT molecules. As shown in Fig. 2 *a*, *E* varied substantially from cell to cell, in this experiment from 10% to over 30%, and was high in cells expressing high amounts of 5′ NT at the apical plasma membrane.

The cell-to-cell variation in *E* contains information about the distribution of 5′ NT molecules on the cell surface (see Table I, test *3*). To obtain this information, we sampled the average values of *E*, acceptor fluorescence intensity, and donor fluorescence intensity after acceptor photodestruction, from 40 × 40-pixel square regions of interest on individual cells (Fig. 1 *c*, *box*). This area represented ~1/5 at 63× or 1/15 at 100× of the projected surface area of a cell of ~100 μm^2. The relationship between

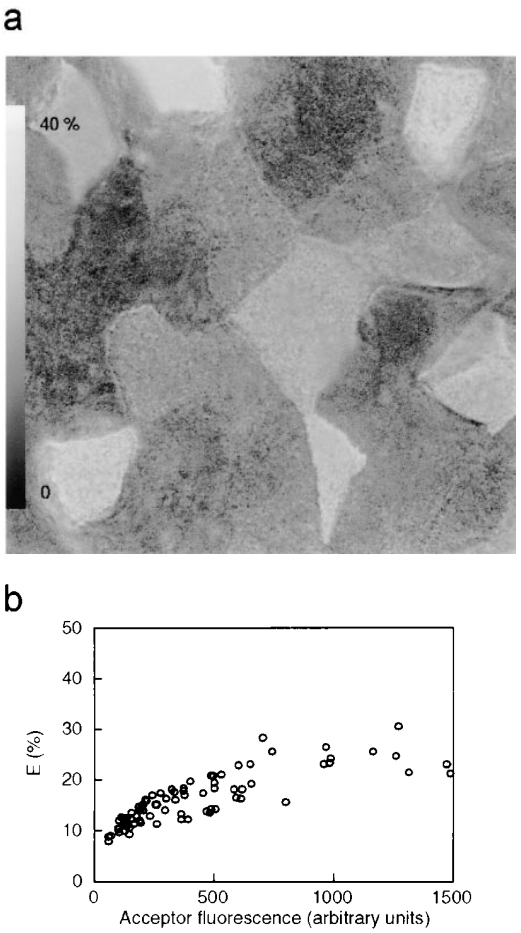

Figure 2. *E* increases with increasing 5′ NT surface densities. (*a*) *E* image calculated from the donor images in Fig. 1 using Eq. 2. The bar indicates the scale for the *E*. (*b*) Graph of *E* (%) versus acceptor fluorescence intensity. Each datum represents the mean *E* and acceptor fluorescence value obtained for a 40 × 40-pixel square region of interest on an individual cell (as described in the Materials and Methods) for the cells in *a* plus three additional fields of cells.

E and acceptor fluorescence for the cells shown in Fig. 1 is shown graphically in Fig. 2 *b*. Each datum represents the mean *E* and acceptor fluorescence taken from one of the cells in the field. Since the acceptor fluorescence (though reported in arbitrary units) is proportional to the relative surface density (number of proteins per unit area) of 5′ NT, Fig. 2 *b* shows that *E* increased as a function of increasing surface density of 5′ NT molecules.

Energy Transfer between Labeled 5′ NT Molecules Scales with the Acceptor Surface Density

Depending on the distribution of donor- and acceptor-labeled molecules, *E* may depend on the surface density of donor and/or acceptors, the extent of labeling, and D:A (Table I and Appendix). In our experiments, the surface density of 5′ NT varied from cell to cell because the cells differed in their expression of the protein (Fig. 1). The surface density of donors and acceptors could be changed by varying D:A, the ratio of donor- and acceptor-labeled antibodies used to label the cells. We expected that for 5′ NT randomly distributed on the cell surface, energy transfer between labeled 5′ NT would scale with the surface density of acceptor, regardless of the way in which the surface density of acceptor was varied. That is, we expect similar values of energy transfer for cells with a high surface density of 5′ NT but labeled with a low concentration of acceptor-conjugated antibody, and for cells with a low surface density of 5′ NT but labeled with a high concentration of acceptor antibody, as long as the acceptor surface density is the same in each cell group of cells (Table I, Fig. 1, 2). Energy transfer was not expected to scale with surface density if 5′ NT was exclusively distributed in clusters (Table I).

Fig. 3 shows the experimental dependence of *E* on D:A, donor surface density, and acceptor surface density. When cells were labeled with a constant molar concentration of donor-labeled IgG, with increasing concentrations of acceptor-labeled IgG to give D:A ranging from 1:0.5 to 1:5. It can be seen that for a single D:A, energy transfer increased with increasing 5′ NT surface density, measured in terms of either donor (Fig. 3 *a*) or acceptor (Fig. 3 *b*) fluorescence, and went to zero in the limit of low surface densities. This dependence of *E* on surface density is inconsistent with a model in which all surface 5′ NT is in clusters (Table I).

For a given donor surface density (Fig. 3 *a*), *E* increased as D:A increased from 1:0.5 to 1:5. This is apparent in the bifurcation of the data curves in Fig. 3 *a*. In contrast, for a given acceptor surface density (Fig. 3 *b*), *E* was approximately the same at all the D:A examined. We also note that the shape of the experimental curves was similar to that predicted for randomly distributed molecules (Fig. 2), although they cannot be directly compared here because the acceptor surface density and *r* are not known (see below for an estimate).

The strong dependence of *E* on the acceptor surface density, but not donor surface density, is consistent with the theoretical prediction for donors and acceptors randomly distributed in the plane of the membrane (Fig. 2). However, this independence of *E* on donor surface density only holds in the limit where there are few donors in the excited state compared with the number of acceptors present (Fung and Stryer, 1978). Consistent with this, we found that if cells were labeled with a constant concentration of acceptor (50 μg/ml) and varying amounts of donor to yield the indicated D:A, energy transfer actually decreased as the concentration of donor was increased to

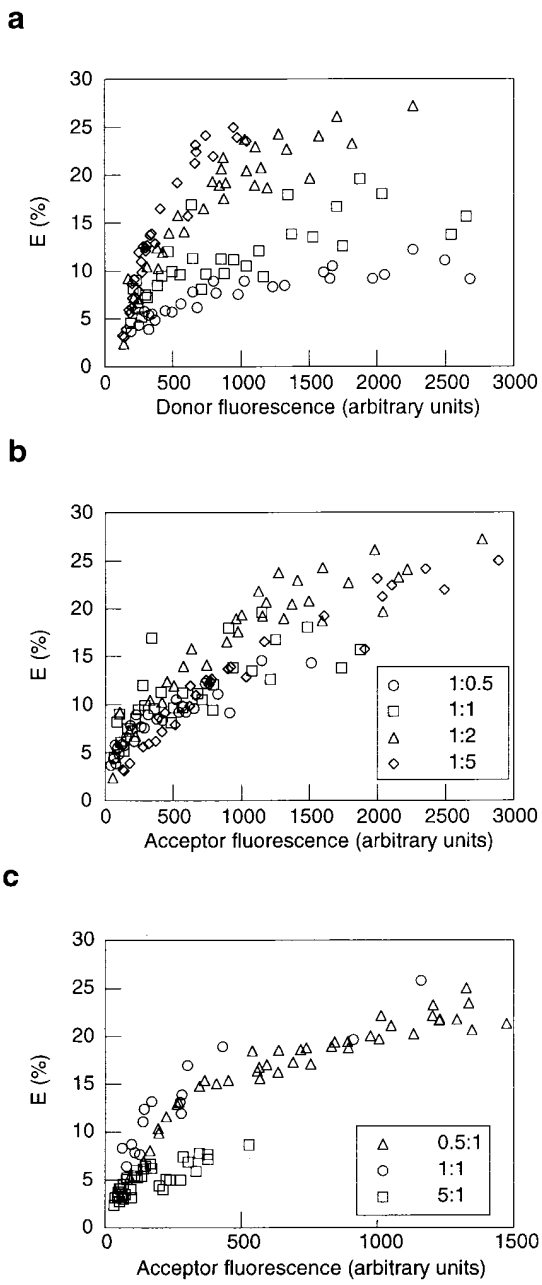

Figure 3. *E* depends on acceptor surface density and is insensitive to D:A, in the regime of low donor surface density, for cells labeled with donor- and acceptor-conjugated IgG. (*a*) *E* as a function of the donor fluorescence, for D:A of 1:0.5 (*circles*), 1:1 (*squares*), 1:2 (*triangles*), or 1:5 (*diamonds*). (*b*) *E* as a function of the acceptor fluorescence, for D:A of 1:0.5 (*circles*), 1:1 (*squares*), 1:2 (*triangles*) or 1:5 (*diamonds*). (*c*) *E* as a function of acceptor fluorescence, for D:A of 0.5:1 (*triangles*), 1:1 (*circles*), or 5:1 (*squares*). Note that in this experiment, the acceptor concentration, rather than the donor concentration, was held constant.

yield D:A of 5:1 (Fig. 3 *c*). For samples labeled with low concentrations of donor (D:A of 0.5:1 and 1:1), the data were similar to those described above (Fig. 3 *b*). Therefore, in all our experiments, samples for FRET were labeled with a constant low concentration of donor (50 μg/ml) and varying concentrations of acceptor.

We considered the possibility that the bivalent IgG used to label 5′ NT may disrupt its normal membrane distribution. To test this, we repeated the experiments in Fig. 3, *a* and *b*, using cells labeled with a monovalent Fab. Fig. 4 shows the results of such an experiment. As above, cells were labeled with a constant amount of donor and with increasing amounts of acceptor. The pattern of immunofluorescence labeling was similar for cells labeled with IgG and Fab (data not shown). As we had observed for the IgG-labeled samples, *E* as a function of acceptor surface density was approximately the same for all D:A (Fig. 4 *b*). However for the Fab-labeled samples, a small but systematic increase in *E* was observed with increasing concentrations of acceptor. In an experiment where we directly compared the magnitude of *E* at a given acceptor fluorescence intensity for samples labeled with IgG versus Fab, we found that *E* was higher for the Fab-labeled samples (data not shown). This is most likely due to differences in the dye/protein ratio for the acceptor-labeled molecules (4.1 for Fab vs 1.7 for IgG), but it could also be due to differences in the size and/or the relative flexibility of Fab and IgG (Kam et al., 1995; Matko and Edidin, 1997). These factors may also account for the increase in *E* with increasing concentration of acceptor-Fab.

We also made FRET measurements in cells that had not been incubated with butyrate, but which nevertheless displayed detectable amounts of 5′ NT. These experiments were done for two reasons. First, we wanted to further test the dependence of *E* on 5′ NT surface density to see whether *E* extrapolated to zero at low surface densities (Table I). Second, the butyrate treatment used to induce high expression of 5′ NT could create artifacts because of overexpression of the protein. For instance, the enrichment of 5′ NT in microdomains in butyrate-treated cells may be limited by the availability of other components of the putative microdomains. Consistent with the lower surface densities of 5′ NT, we found that *E* was correspondingly lower on the untreated cells (data not shown and Figs. 6 and 7). As we had found for the butyrate-treated cells, at a given acceptor surface density *E* was similar at all D:A examined (data not shown). This suggests that the distribution of 5′ NT is not affected by the level of expression of the protein.

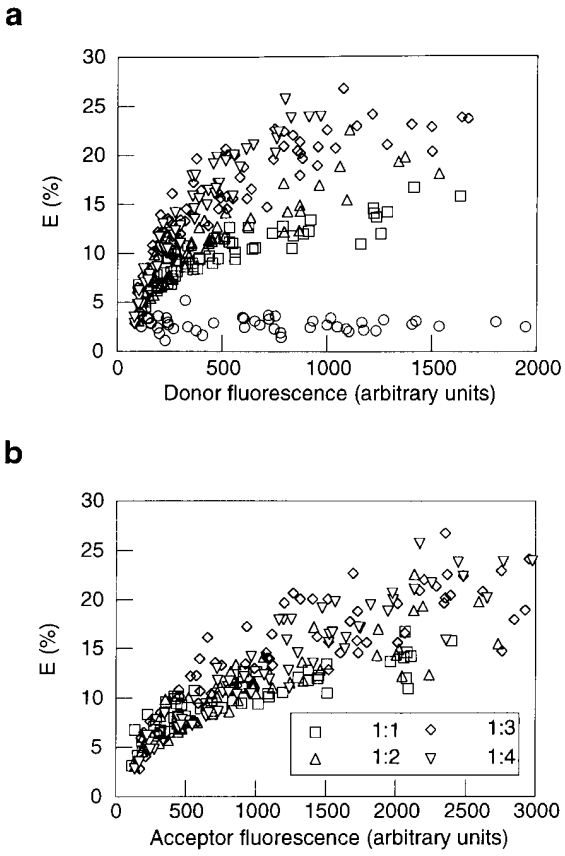

Figure 4. *E* depends on acceptor surface density for cells labeled with donor- and acceptor-conjugated Fab. (*a*) *E* as a function of the donor fluorescence, for D:A of 1:0 (*circles*), 1:1 (*squares*), 1:2 (*triangles*), 1:3 (*diamonds*), or 1:4 (*inverted triangles*). (*b*) *E* as a function of the acceptor fluorescence, for D:A of 1:1 (*squares*), 1:2 (*triangles*), 1:3 (*diamonds*), or 1:4 (*inverted triangles*).

Energy Transfer between Labeled 5′ NT Falls in the Range Predicted for High Surface Densities of Randomly Distributed Donor and Acceptors

In the experiments described above, the acceptor surface densities were presented in arbitrary units; hence, we could not directly compare the experimental data with theoretical predictions. To compare experimental data with theoretical predictions, we estimated absolute surface densities of acceptors on cell membranes from the measured fluorescence intensities using a set of calibration standards, 8-μm-diam beads with known antibody binding capacities. Fig. 5 compares the experimental values of *E* plotted as a function of absolute acceptor surface density (Fig. 5 *a*), with the theoretical values of *E* for randomly distributed donors and acceptors (Fig. 5 *b*). We estimated maximum acceptor surface densities of 20,000 per μm^2 (Fig. 5 *a*). These values are high and may be overestimates, but they are not unprecedented (Rothberg et al., 1990; Hille, 1992). The theoretical curves (Fig. 5 *b*) were calculated for values of closest approach, *r*, ranging from $r = 0$, where the donor and acceptor are in physical contact, to $r = 2R_o$, where the closest possible approach of the donor and acceptor is constrained to 100 Å. If *r* is approximated by the diameter of the donor- and acceptor-labeled molecules (Zimet et al., 1995), $r = 1.5R_o$ would be roughly comparable to the size of an Fab, which has been estimated as a cylinder with a diameter of 80 Å and a height of 70 Å (Kubitscheck et al., 1993).

A comparison of Fig. 5, *a* and *b*, shows that the overall shapes of the experimental and theoretical curves are similar, and that the experimental data fall within the range of the theoretical predictions. The experimental data are similar to the theoretical curves for $r = 0$ at low surface densities, and $r = 1.5R_o$ at high surface densities. Though this variation in *r* as a function of surface density may reflect the biology of 5′ NT, it may also result from errors in the estimate of the acceptor surface density and from the fact

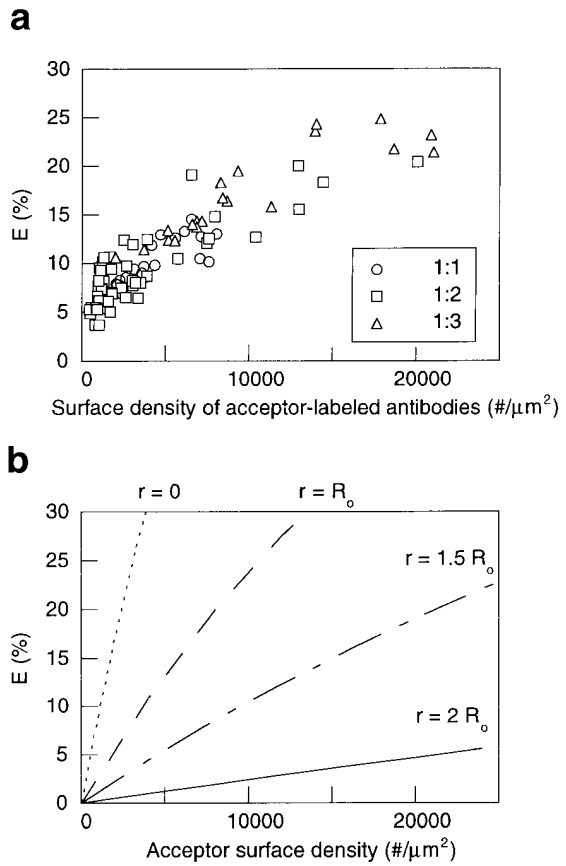

Figure 5. Experimental energy transfer efficiencies are similar to those predicted for randomly distributed donors and acceptors when plotted as a function of absolute acceptor surface density. (*a*) Data from the experiment in Fig. 2 plotted in terms of absolute acceptor-labeled antibody surface density, estimated using fluorescent calibration standards as described in the Materials and Methods, for D:A of 1:1 (*circles*), 1:2 (*squares*), and 1:3 (*triangles*). (*b*) Theoretical curves from Fig. A2 were replotted in terms of absolute acceptor surface densities, assuming R_o = 50 Å. Curves were calculated using the third approximant of Dewey and Hammes (1980) for $1.5R_o$ and $2R_o$ or Eq. A1 (Wolber and Hudson, 1979) for $r = 0$ and $r = R_o$.

that the theoretical calculations assume one fluorophore per protein molecules, while our Fab and IgG labels carry two or more fluorophores per molecule.

Energy Transfer between Labeled Primary and Secondary Antibodies Is a Positive Control for "Clustering"

As a direct test of whether our method could detect clustered molecules, we measured energy transfer from donor-labeled anti–5′ NT Ig to acceptor-labeled anti-Ig antibodies. Direct binding of the secondary antibodies to the primary antibodies should lead to relatively high values of E, and E should reflect the combined contributions of "clustered" (directly bound) and randomly distributed molecules (Appendix). We expect that this system should behave as a mixture of randomly distributed and clustered molecules, where $f_{clustered}$ is constant (Table I, Fig. A3, *a* and *b*). Although at first it might appear that since the acceptors bind donors that this should instead be equivalent to the model presented in Fig. 3 *c*, this is not the case because in our experiment, the ratio of primary and secondary antibodies bound to any given cell, and thus $f_{clustered}$, is constant.

As expected, for samples labeled with donor-conjugated primary and acceptor-conjugated secondary antibodies, the amount of secondary antibody bound to any given cell was directly proportional to the amount of primary antibody bound, and thus proportional to the surface density of 5′ NT (data not shown). Compared with a control sample labeled with donor- and acceptor-conjugated primary antibodies, significantly higher values of E were observed for the samples labeled with the donor-conjugated primary and acceptor-conjugated secondary antibodies (Fig. 6). Moreover, in the clustered samples, E increased as the concentration of acceptor-conjugated secondary antibody used to label the cells was increased. In this experiment, E increased from a maximum of ~20% to a maximum of close to 40%, as D:A was increased from a nominal ratio of 1:0.1 to 1:1. For comparison, an E of 28% has been measured between the A- and B-subunits of the intact structure of cholera toxin, molecules in molecular contact (Bastiaens et al., 1996).

The increase in E observed as the concentration of acceptor in D:A was increased could reflect an increase in the fraction of donors to which acceptors were bound ($f_{clustered}$ in Eq. A5), an increase in the number of acceptors (secondary antibodies) bound per donor ($E_{clustered}$ in Eq. A5), or both. E for the clustered molecules also showed some dependence on the acceptor surface density. This is probably due to intercluster energy transfer. Note especially that at the lowest surface densities observed, E for the control sample was less than 5%, compared with >10% or >20% for the samples labeled with 5 or 50 μg/ml of acceptor-labeled secondary antibody, respectively.

Energy Transfer Is Enhanced by Secondary Antibody Cross-Linking or by Detergent Extraction

GPI-anchored proteins on cell surface can be clustered by cross-linking with secondary antibody (Mayor et al., 1994;

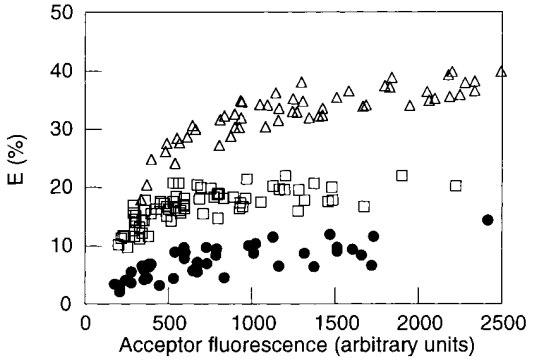

Figure 6. Positive control for "clustered" donors and acceptors: energy transfer between donor-labeled primary antibodies and acceptor-labeled secondary antibodies. Uninduced cells were labeled either with 1:1 D:A (IgG) as in previous experiments (*closed circles*) or with 50 μg/ml of Cy3 anti–5′ NT IgG for 15 min at 4°C, washed, and then labeled for 15 min at 4°C with either 5 μg/ml (*squares*) or 50 μg/ml (*triangles*) Cy5-labeled donkey anti–mouse IgG, washed, and then fixed as previously described.

Fujimoto, 1996) or by detergent extraction of cells (Mayor and Maxfield, 1995). If this clustering also occurs over molecular length scales, it ought to cause a detectable change in the energy transfer between labeled 5′ NT molecules.

To cluster 5′ NT with secondary antibody, cells were labeled with donor- and acceptor-conjugated antibody followed by an anti-IgG secondary antibody and a brief incubation at 37°C. With this treatment, the label clustered into large punctate structures (Fig. 7 *c*). For a given acceptor surface density, higher values of *E* were observed in cells labeled with secondary antibody than in control cells (Fig. 7 *e*). This difference was not very large, in part because, for the clustered sample, *E* is an average for the areas depleted and enriched in 5′ NT (Fig. 7 *d*). This finding is consistent with a report that the average *E* for cells labeled with donor- and acceptor-labeled Concanavalin A was similar under conditions where the label was ring-stained and when it was patched (Dale et al., 1981).

5′ NT is found in low-density, detergent-insoluble membrane microdomains in intestinal epithelial cells (Strohmeier et al., 1997) and rat lung endothelial cells (Schnitzer et al., 1995). To see if Triton X-100 extraction changed the organization of 5′ NT in intact MDCK cell membranes, living cells were labeled at 4°C with donor- and acceptor-labeled antibodies and then incubated on ice with 1% Triton X-100 for 30 min before fixation. As reported for other GPI-anchored proteins (Mayor and Maxfield, 1995), 5′ NT was not significantly solubilized under these conditions, since the intensity and pattern of its labeling were very similar to control cells (Fig. 8). However, in some

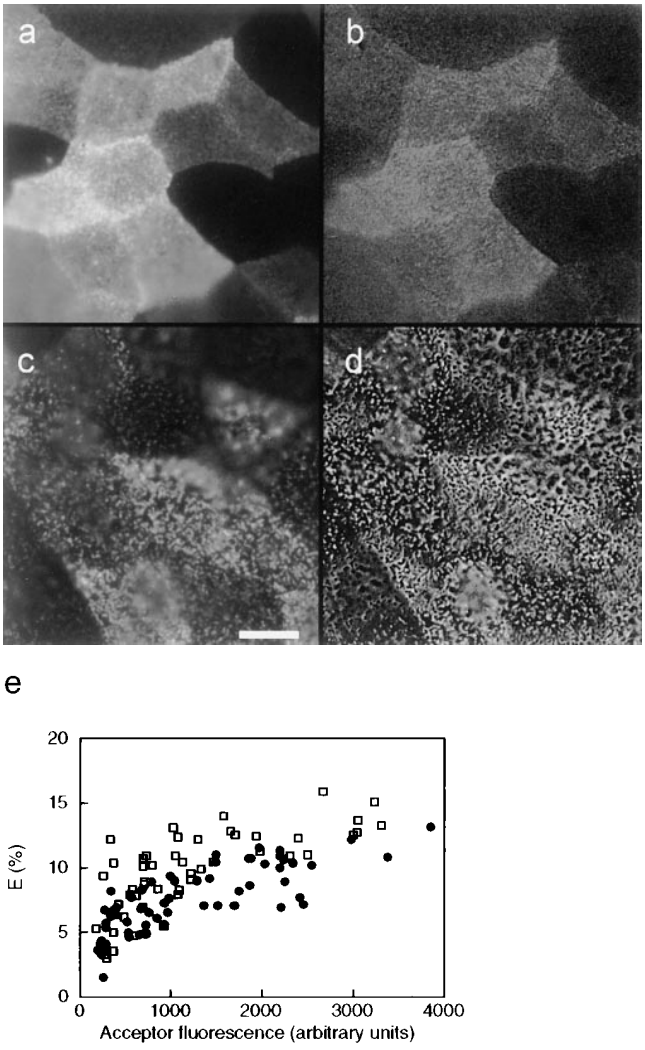

Figure 7. Energy transfer between anti–5′ NT antibodies is enhanced by antibody-induced cross-linking. Acceptor fluorescence images (*a* and *c*) and *E* images (*b* and *d*) of uninduced cells (expressing low levels of 5′ NT) labeled with 1:1 D:A (IgG) followed by an incubation in the absence (*a* and *b*) or presence (*c* and *d*) of 10 μg/ml unlabeled secondary antibody. (*e*) *E* as a function of acceptor fluorescence for cells labeled with 1:1 D:A (IgG) in the presence (*open squares*) or absence (*closed circles)* of secondary antibody. Bar, 10 μm.

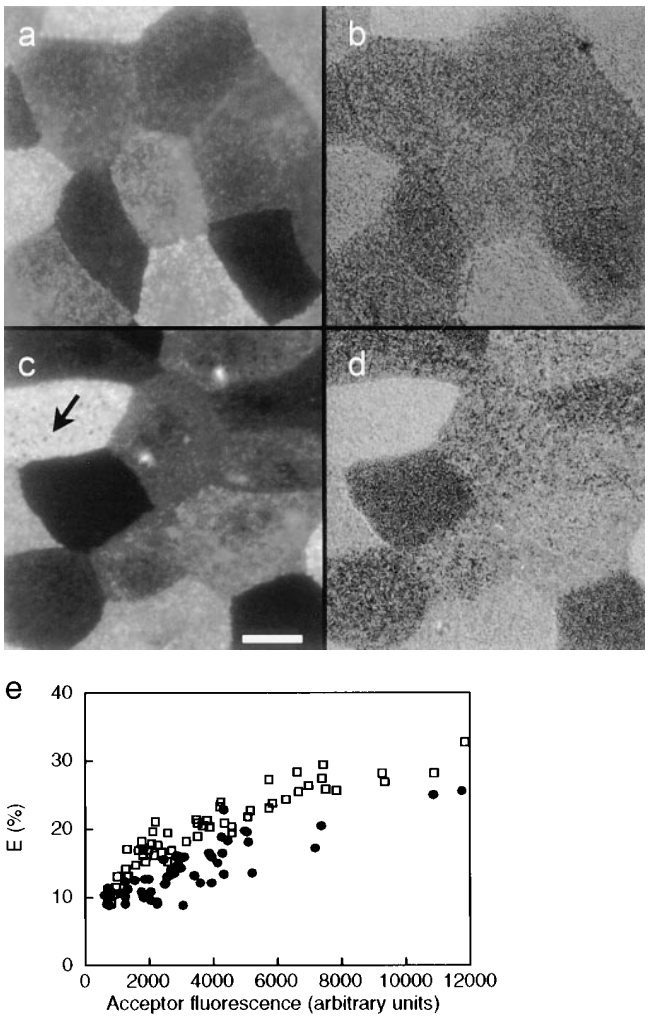

Figure 8. Energy transfer between anti–5′ NT antibodies is enhanced by Triton X-100 extraction of cells. Acceptor fluorescence images (*a* and *c*) and *E* images (*b* and *d*) of cells induced to express high levels of 5′ NT, labeled with 1:1 D:A (Fab) followed by a 30-min incubation at 4°C in PBS^{++} (*a* and *b*) or PBS^{++} containing 1% Triton X-100 before fixation (*c* and *d*). The arrow in *c* points to a hole in the membrane, formed by the Triton X-100 extraction procedure. (*e*) *E* as a function of acceptor fluorescence for cells incubated in the presence (*open squares*) or absence (*closed circles*) of 1% Triton X-100. Bar, 10 μm.

cells, dark unlabeled regions in the membrane (presumably holes) were apparent, indicating that other membrane components had been solubilized (Fig. 8 *c*, *arrow*). *E* measured after detergent extraction was systematically higher than controls, consistent with a shift to a partially clustered distribution of 5′ NT after detergent extraction (Fig. 8 *e*).

These results suggest that not all 5′ NT was clustered after secondary antibody labeling or detergent extraction, but instead was present as a mixture of randomly distributed and clustered molecules. To this point, it is important to note that changes (or lack thereof) in the apparent organization of the protein at the light or even the electron microscopic level may not be directly correlated with changes detected by FRET, since they measure distances over different length scales (c.f., Damjanovich et al., 1995).

Discussion

Membrane microdomains enriched in GPI-anchored proteins, GSL, and cholesterol have been operationally defined in terms of detergent-insoluble, low-density membrane fractions; however, these microdomains have not been detected by other techniques (for review see Harder and Simons, 1997). In the present study, we used imaging FRET, a method that increases the resolution of immunofluorescence microscopy to the molecular scale, to probe for microdomains enriched in a GPI-anchored protein in the apical plasma membrane of MDCK cells. We expected that if most of the GPI-anchored protein 5′ NT was in membrane microdomains, then we would be able to detect FRET between 5′ NT molecules that was consistent with clustering (Table I).

Using imaging FRET, we obtained images that showed significant cell-to-cell variation in efficiencies of energy transfer between labeled 5′ NT molecules. *E* strongly correlated with the surface density of 5′ NT and approached zero at low surface densities (Figs. 3–6). These observations suggest that most of 5′ NT is not in clusters at the apical membrane of MDCK cells; if it were, we would have expected to measure high *E* even at low surface densities (Table I). These observations were not due to the failure of the method to detect clusters since we detected clustered donors and acceptors in a simple model system, secondary antibodies bound to primary antibodies (Fig. 6).

The distinct dependence of *E* on the surface density of 5′ NT (Figs. 3–6) is consistent with either an entirely random distribution of the protein or a mixture of randomly distributed and clustered 5′ NT (Table I). If some 5′ NT is in clusters and some is randomly distributed, we expect that *E* will not necessarily go to zero in the limit of low surface densities, and *E* will be sensitive to D:A (Table I). If little or no 5′ NT is in clusters, then we expect *E* to go to zero in the limit of low surface density to be insensitive to D:A.

We found that *E* approached zero in the limit of low 5′ NT surface densities (Figs. 3-6), and the shape of the experimental curves was similar to that predicted theoretically for a random distribution (Fig. 5). *E* depended strongly on the surface density of acceptor, and not of the surface density of donors for relatively low concentrations of the donor fluorophore. Regardless of D:A, data from an individual experiment tended to fall on a single curve when plotted as a function of acceptor surface density in cells expressing widely varying concentrations of protein (Fig. 3). However, in some experiments (Fig. 4) we observed small shifts in *E* for samples labeled with different D:A ratios, which hints that some clusters may be present. We thus cannot completely rule out the possibility that though most are randomly distributed, some 5′ NT molecules are clustered. We expect that under some circumstances, FRET for mixtures of randomly distributed and clustered molecules will appear similar to FRET for a purely random distribution, particularly in the limit where $f_{\text{clustered}}$ and/or $E_{\text{clustered}}$ is small, and f_{random} and/or E_{random} is large (see Appendix). This could explain for instance why we did not observe a larger effect on *E* in cells where we induced clustering of GPI-anchored proteins by secondary antibody-induced cross-linking, or by detergent extraction of intact cells (Figs. 7 and 8). We calculated that if 10% of the molecules were clustered, data for a mixed population would appear very similar to a pure random distribution (assuming $r = R_o$). However, large differences are expected when $f_{\text{clustered}} = 50\%$ (see Appendix). Based on these observations, the simplest interpretation of our data is that 5′ NT is predominantly randomly distributed under the conditions of our experiments.

It is important to emphasize that our conclusion that 5′ NT is predominantly randomly distributed depends on the presence of FRET and not its absence. In a previous study from our laboratory, no FRET was detected between labeled gD1-DAF molecules under steady-state condition, implying that gD1-DAF was dispersed, i.e., randomly distributed (Hannan et al., 1993). However, the absence of FRET does not necessarily eliminate the possibility that molecules are clustered together, since among other possibilities the distance separating them in the cluster may be larger than can be detected by FRET. In the present study we were able to detect FRET between labeled 5′ NT molecules; this indicates that, on average, the proteins are already within 10's of Å of one another. This provides further evidence that FRET would be able to detect enrichment of 5′ NT in microdomains, i.e., lipid rafts. Reexamination of the lateral organization of gD1-DAF using our current FRET method shows that energy transfer is detected between labeled gD1-DAF molecules under steady-state conditions and is correlated with protein surface density, similar to our results for 5′ NT (Nguyen, T., A. Kenworthy, and M. Edidin, unpublished observations). The difference between our past and present results may be due to lower concentrations (surface densities) of labeling antibodies in our previous experiments, and the sensitivity of the current method to cell-to-cell variations in *E*. This further emphasizes the most important advantage of imaging FRET over nonimaging FRET experiments, which typically yield average *E* values for a population of cells (Hannan et al., 1993; Matko and Edidin, 1997): imaging FRET generates images mapping energy transfer efficiencies. Although in the current study we have focused on protein homoassociations, imaging FRET is also uniquely suited for performing "imaging biochemistry" of protein–protein and protein–lipid heterointeractions in intact cells.

To further verify our conclusion that most 5′ NT is randomly distributed in the cell surface would require a quantitative comparison of our data with the theoretical predic-

tions. Variations on the analytical approach we applied here have been used to quantitatively interpret FRET data in a variety of membrane systems (e.g., Holowka and Baird, 1983*a*,*b*; Dewey and Datta, 1989; John and Jähnig, 1991; also see Mátyus, 1992 and Clegg, 1996 for a more comprehensive list). However, our ability to extend our current analysis from a qualitative to a quantitative one is limited by several factors. First, there is some spread in the energy transfer versus acceptor surface density curves that could mask differences in the data sets. Factors contributing to this variability include inhomogeneities in the excitation across the field of view, small local variations in quenching of donor, and the inherent heterogeneity of fluorescence labeling pattern of the cell surface due to the presence of microvilli and the curvature of the apical membrane itself. Second, the lower limit of detectability of FRET with our method is conservatively 5%, although in many experiments we measured apparent E for negative controls (labeled with donor only) of as low as 2–3% (Fig. 4). This could be further improved by additional background subtraction. In the current experiments, because we were imaging confluent monolayers of cells, the only background subtraction we included was for the so-called dark current, a constant contribution due to noise from the CCD camera. With higher sensitivity we could estimate the extrapolation of E and the acceptor surface density to zero with greater confidence. Third, there are limits to our comparisons of experimental results to theory and with the theoretical calculations themselves. Our ability to rigorously test the theoretical predictions would be improved by better estimates of acceptor surface density and r. A physically based approximation of r, for instance, would require more detailed structural information about 5′ NT, including the position of the epitope and the orientation of the bound antibody. To this point, we note that a number of sophisticated analyses have been developed that incorporated detailed information about the experimental system, such as the position of the donor fluorophore on the molecule of interest (e.g., Zimet et al., 1995). This kind of information could be usefully applied in the analysis of imaging FRET data for better characterized experimental systems. The analysis would also be improved by better theoretical models for mixed populations, including specific cross-terms between the randomly distributed and clustered molecules.

It is well known that the distribution of GPI-anchored proteins in cell membranes is sensitive to fixation and labeling conditions. For example, GPI-anchored folate receptor was reported to be clustered (Rothberg et al., 1990), but this was subsequently shown to be induced by cross-linking of secondary antibodies (Mayor et al., 1994). Clustering of 5′ NT itself has also been shown after antibody cross-linking (Howell et al., 1987). In our experiments, we observed very similar, dispersed labeling patterns produced by either monovalent Fab or bivalent IgG when the cells were directly fixed after labeling. In addition, the organization of the primary antibodies became more punctate (clustered) in the presence of secondary antibodies (Fig. 7 and data not shown). Thus, our results are similar to previous reports in this regard (Rothberg et al., 1990; Mayor et al., 1994). However, very recent work suggests that certain fixation conditions may act to disperse preexisting clusters of the folate receptor (Wu et al., 1997), reopening the question of how to best stabilize the native distribution of GPI-anchored proteins. This issue will require further study. Nevertheless, our current results are consistent with reports (Parton et al., 1994; Mayor and Maxfield, 1995; Fujimoto, 1996; Rijnboutt et al., 1996) of predominantly random steady-state distributions of GPI-anchored proteins, measured at the level of resolution of the electron microscope. Compared with electron microscopy, imaging FRET has the advantages of higher labeling efficiency, a larger sample size, and most importantly, increased resolution, to the molecular level.

The first experimental evidence for the existence of membrane microdomains enriched in GPI-anchored proteins was the isolation, as buoyant complexes, of detergent-insoluble membrane fractions enriched in GPI-anchored proteins, GSL, and cholesterol from MDCK cells (Brown and Rose, 1992). The GPI-anchored protein PLAP was found to become detergent insoluble in the Golgi, a property that persisted even after the protein reached the apical membrane (Brown and Rose, 1992). Additional components of detergent-insoluble membrane microdomains were later shown to include signal-transducing lipid-modified proteins such as nonreceptor tyrosine kinases and the caveolar marker caveolin (Stefanova et al., 1991; Sargiacomo et al., 1993;Arreaza et al., 1994; Melkonian et al., 1995). Recently, a number of studies have helped clarify the relationship between membrane microdomains enriched in GPI-anchored proteins, detergent-insoluble complexes, and caveolae, 70–100-nm invaginations of the plasma membrane that are decorated with the protein caveolin (Fra et al., 1994; Schroeder et al., 1994; Gorodinsky and Harris, 1995; Mayor and Maxfield, 1995; Schnitzer et al., 1995, 1996; Smart et al., 1995; Hannan and Edidin, 1996; Ahmed et al., 1997). These studies indicate that proteins and lipids that share the common property of detergent insolubility are not necessarily associated in intact cell membranes, but leave open the question of the size and nature of the microdomains before detergent extraction (Kurzchalia et al., 1995; Edidin, 1997; Harder and Simons, 1997; Weimbs et al., 1997). There is clearly a need for a more precise definition of what constitutes a functional membrane microdomain in intact cell membranes.

Our findings, obtained using a high-resolution imaging technique, begin to place distinct limits on the structure of microdomains enriched in GPI-anchored proteins in intact cell membranes. We report here that the GPI-anchored protein 5′ NT, which is known to associate with detergent-insoluble complexes (Mescher et al., 1981; Schnitzer et al., 1995; Strohmeier et al., 1997), is also resistant to Triton X-100 extraction in MDCK cells. Yet it appears that most 5′ NT are randomly distributed and are not clustered over the <100-Å length scale of the FRET measurements. This places limits on the ways in which GPI-anchored proteins can associate with lipid rafts. For example, our data argue against a model where 5′ NT is predominantly associated with a finite number of rafts, since we would have expected to measure relatively high energy transfer because of clustering of the protein in rafts, even at low surface densities of 5′ NT expression (Fig. 3). The limitations of our current measurements prevent us from ruling out the

possibility that FRET between 5′ NT arises from a mixture of a large fraction of randomly distributed and a small fraction of clustered (raft-associated) molecules. However, it is interesting to consider the consequence of a purely randomly distribution of 5′ NT for the structure of lipid rafts. If this were the case, then these membrane microdomains must either be vanishingly small (in agreement with a current model [Harder and Simons, 1997]), or alternately must comprise the entire apical membrane. Our results also have implications for the membrane organization of GPI-anchored proteins during membrane trafficking and sorting, since the biochemical properties of the membrane microdomains involved in sorting and the steady-state organization of GPI-anchored proteins are assumed to be similar. This could be further tested by directly examining the membrane organization of GPI-anchored proteins and other apically destined proteins and lipids in the Golgi. Further work will be also be required to determine whether functional associations of other lipid-modified proteins and GSL can be visualized in cell membranes, and whether these associations are mediated by lipid–lipid or protein–lipid interactions. Imaging FRET will be a powerful tool to further investigate these questions in intact cells.

Appendix

Theoretical Dependence of FRET on the Distribution of Donor- and Acceptor-labeled Molecules in Membranes

FRET detects the proximity of donor- and acceptor-labeled molecules over distances of <100 Å (Eq. 1). FRET can be used to study the distribution of molecules in membranes because the average spacing between molecules of interest will depend primarily on their lateral distribution (Fig. A1). Molecules may be within FRET distance either because they are clustered or because they are randomly distributed at surface densities high enough so that there is a fraction of randomly distributed labeled molecules in FRET proximity. The basis for FRET can be determined by considering predictions of theoretical models for FRET between clustered or between randomly distributed molecules. Below we consider the predictions for three models of proteins labeled with a mixture of donor and acceptor fluorophores: randomly distributed molecules, entirely clustered molecules, and a mixture of randomly distributed and clustered molecules. We show that we can distinguish between the models by determining the dependence of E on the total surface density of the molecules of interest and the mole ratio of donor to acceptors (D:A) used to label them.

Randomly Distributed Donors and Acceptors

For randomly distributed donors and acceptors in membranes, the energy transfer efficiency E_{random} is a function of R_o, r, and the surface density of acceptors (Shaklai et al., 1977; Fung and Stryer, 1978; Wolber and Hudson, 1979; Dewey and Hammes, 1980; Snyder and Freire, 1982; Yguerabide, 1994). Here, r is defined as the distance of closest potential approach of the donors and acceptors. This takes into account the fact that donors and acceptors are attached to molecules, proteins or lipids, that have some finite size. A typical value of r for energy transfer between small lipid probes is ~10 Å (Dewey and Hammes, 1980). For protein–protein interactions, r can be approximated by the protein diameter, for instance, ~40 Å for calcium ATPase (Dewey and Datta, 1989; Zimet et al., 1995).

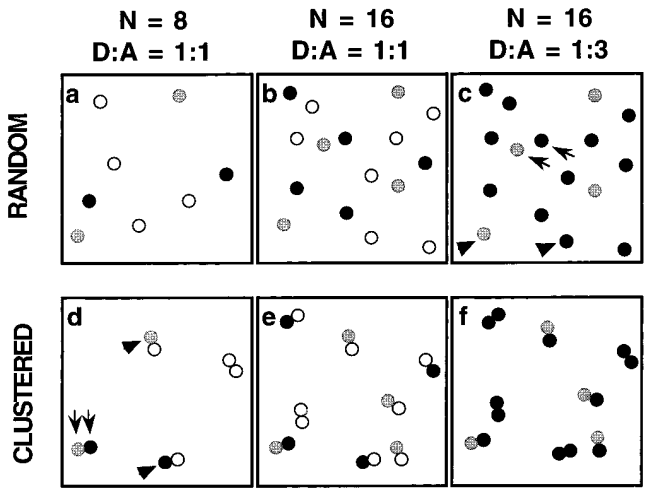

Figure A1. Schematic depiction of how surface density of proteins and D:A differently influence FRET for randomly distributed (*a–c*) and clustered (*d–f*) molecules on a membrane. For simplicity, "clustered" molecules are modeled as the minimal form of clusters, dimers. The molecules of interest are either unlabeled (*open circles*) or labeled with donor (*gray circles*) or acceptor (*black circles*) to yield the indicated D:A. For each condition, the area of the membrane examined (*box*) is held constant, and the surface density is varied by changing the number N of molecules per box. The size of the molecules of interest determines the scale of the model. For instance, if we assume a particle diameter of 5 nm (50 Å), then the box size is 70 × 70 nm. The arrows in *c* and *d* indicate a donor and acceptor pair that are in close enough proximity for energy transfer to occur at this scale, and the arrowheads point to a donor and acceptor pair that are too far apart for energy transfer to occur. Note that because we only show a limited number of molecules, these models are not statistically accurate. For example, the apparent $E_{\text{clustered}}$ for the model in *f* is 50%, but for an experimental population labeled at this D:A, $E_{\text{clustered}}$ would be 37.5%, as described in the text.

The equation relating E_{random}, r, R_o, and acceptor surface density is in a form that must be solved numerically, and thus a number of analytical approximations of this equation have been developed (Shaklai et al., 1977; Wolber and Hudson, 1979; Dewey and Hammes, 1980; Snyder and Freire, 1982; Yguerabide, 1994). Two approximations that together accurately span a useful range of values of r are from Dewey and Hammes (1980) and Wolber and Hudson (1979). The approximation of Wolber and Hudson (1979) is

$$E_r = 1 - \left(A_1 e^{-k_1 c_A} + A_2 e^{-k_2 c_A} \right), \quad \text{(A1)}$$

where c_A is the so-called reduced acceptor surface density, a dimensionless parameter equal to R_o^2 multiplied by the acceptor surface density, and $A_{1,2}$ and $k_{1,2}$ are constants that are different for different values of r. Dewey and Hammes (1980) derived fractional approximations for E_{random}, the first of which is given by

$$E_{\text{random}} = 1 - \{1 + [(\pi c_A/2)\ (R_o/r)^4]\}^{-1}. \quad \text{(A2)}$$

Here again c_A is the reduced acceptor surface density, as defined above. Eq. A1 is valid for $r < 1.3R_o$ and Eq. A2 is valid for $r \geq R_o$. Other limiting conditions are: (*a*) The number of donors must be small enough that donor- donor transfer is negligible; (*b*) the number of donors in the excited state must be small compared with the number in the ground state so that donors do not compete for transfer to a given acceptor; (*c*) r must not change over the excited state lifetime of the donor; and (*d*) all donor–acceptor pairs must have the same R_o (Fung and Stryer, 1978; Wolber and Hudson, 1979; Zimet et al., 1995).

In Fig. A2, we plot Eqs. A1 and A2 as a function of acceptor surface density, for various values of r. E_{random} is dependent on r, reaching its highest potential value as r approaches zero. For any given value of r, E_{random} is zero in the limit of very low acceptor surface densities and increases monotonically with increasing acceptor surface density (Fig. A2). This is because as surface density increases, the distance between adjacent donor- and acceptor-labeled molecules decreases (Fig. A1, *a* and *b*). Although E_{random} is dependent on acceptor surface density, it is independent of donor surface density (Eqs. A1 and A2) since each donor experiences the same average acceptor surface density. (As indicated above, this is only true in the limit where the donor surface density is low enough that excited state donors do not compete for acceptors.) For example, if two samples with the same surface density of protein were labeled with different D:A (Fig. A1, *b* and *c*), E_{random} would be higher for the sample labeled with the higher concentration of acceptors (Fig. A1 *c*). Note also that since E_{random} is only sensitive to the surface density of acceptor-labeled molecules, the presence of unlabeled molecules does not influence E_{random}. Using this information, E_{random} can be estimated for the molecules in Fig. A1 by assigning a scale to the model. For example, if the particle diameter is set as 50 Å ($r = R_o$), then the acceptor surface density in Fig. A1 *c* is 2500/μm^2, yielding an E_{random} of 7% (Eq. A1).

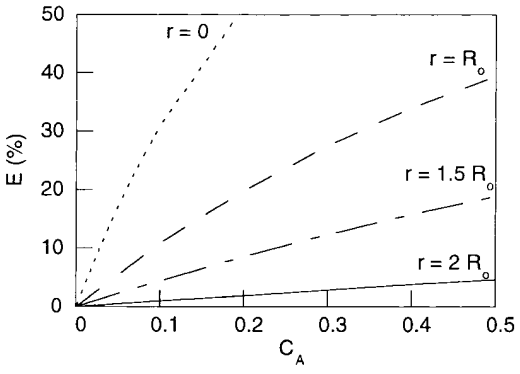

Figure A2. Theoretical dependence of energy transfer efficiency E_{random} on acceptor surface density, r, and R_o for randomly distributed donors and acceptors in a membrane. The acceptor surface density is represented by the dimensionless parameter c_A. Theoretical curves were calculated using the third approximant of Dewey and Hammes (1980) for $r = 1.5R_o$ and $2R_o$ or Eq. A1 (Wolber and Hudson, 1979) for $r = 0$ and R_o, as indicated on the figure.

Clustered Donors and Acceptors

A simple model has been derived to predict the energy transfer efficiency for clustered molecules, $E_{\text{clustered}}$, in the case where the clusters are small well-defined oligomers such as dimers and trimers (Veatch and Stryer, 1977; Adair and Engelman, 1994). This model makes several simplifying assumptions, including the assumption that there are no surface density–dependent interactions between oligomers, and that all of the molecules of interest are oligomerized. Thus, it also assumes that labeling the molecules does not affect their oligomerization. Under these conditions,

$$E_{\text{clustered}} = E_{\text{oligomer}}(1 - f_{\text{DU}}^{\,n-1}). \quad \text{(A3)}$$

Here, n is the number of units in the oligomer, f_{DU} is the total mole fraction of donor-labeled and unlabeled molecules of interest, and E_{oligomer} is the energy transfer efficiency for the oligomer. For the case of dimers ($n = 2$), this simplifies to

$$E_{\text{clustered}} = E_{\text{dimer}} f_A, \quad \text{(A4)}$$

where E_{dimer} is the energy transfer efficiency of a dimer labeled with one donor and one acceptor, and f_A is the mole fraction of acceptor-labeled molecules ($f_A + f_D + f_U = 1$). This model predicts that $E_{\text{clustered}}$ will depend on both D:A and the extent of labeling of the molecules of interest. For example, for two samples with the same surface density of protein (Fig. A1, *e* and *f*), if we assume $E_{\text{dimer}} = 50\%$ and the indicated D:A, then $E_{\text{clustered}} = (50\%)(.25) = 12.5\%$ for Fig. A1 *e*, while $E_{\text{clustered}} = (50\%)(0.75) = 37.5\%$ for Fig. A1 *f*. The cluster model also predicts that $E_{\text{clustered}}$ will be independent of the surface densities of the labeled molecules of interest. Thus, $E_{\text{clustered}} = (50\%)(.25) = 12.5\%$ for two samples with different surface densities but labeled with the same D:A (Fig. A1, *d* and *e*). Based on this prediction, $E_{\text{clustered}}$ would be expected to be nonzero even at low surface densities of the molecule of interest. These properties contrast with the predictions for randomly distributed molecules (Fig. A1, *a–c*), where E_{random} scales strictly with the acceptor surface density (Eqs. A1 and A2).

Although this model may be oversimplified, it provides a useful tool to think about how $E_{\text{clustered}}$ depends on D:A, the extent of labeling, and both donor and acceptor surface density for molecules constrained to a clustered distribution. While the model presented above equates "clustered" molecules with "associated" molecules, this of course is not necessarily the case. In general, to predict $E_{\text{clustered}}$ for more complex clustered distributions would require more specific information about the geometry of the clustered molecules such as the size and shape of the clusters, as well as the position of the fluorescent probe(s) on the molecules of interest. $E_{\text{clustered}}$ would then ultimately depend on the probability of labeling adjacent members of an individual cluster within FRET distance of one another with donors and acceptors.

Mixtures of Clustered and Randomly Distributed Molecules

The simple model for clusters presented above assumes that all of the molecules of interest are associated in clusters. If a mixture of monomeric, randomly distributed mol-

ecules and clustered molecules is present, we would expect two contributions to $E_{mixture}$, one from the randomly distributed fraction of donors and acceptors, and the other from the clustered molecules:

$$E_{mixture} = f_{random}E_{random} + f_{clustered}E_{clustered}, \quad \text{(A5)}$$

where f_{random} and $f_{clustered}$ are the molar fractions of randomly distributed and clustered donors, respectively. E_{random} is the energy transfer efficiency for the randomly distributed molecules (Eq. A1 or A2), and $E_{clustered}$ is the energy transfer efficiency of clustered molecules (for example, from Eq. A4 for dimers). It immediately follows from this equation that because E_{random} is a function of the acceptor surface density (Eqs. A1 and A2), $E_{mixture}$ would also depend on acceptor surface density. Note that for the sake of simplicity, this model does not include any terms that take into account FRET between clusters or between the clustered and randomly distributed molecules. Such interactions would further depend in more complicated ways on $f_{clustered}$, f_{random}, and the surface density of the molecules of interest.

We will consider two limiting cases for the mixed population described by Eq. A5. The first is the case where regardless of overall surface density of the molecules of interest, the mole fraction of randomly distributed and clustered molecules remains constant, in other words, $f_{clustered}$, f_{random}, and $E_{clustered}$ are assumed to be constants. Fig. A3 *a* shows $E_{mixture}$ calculated for two different values of $f_{clustered}$, assuming $E_{clustered}$ = 37.5% (similar to the example given for Fig. A1 *f*). The results of this calculation show that, at a single D:A, when 10% of the molecules are clustered, $E_{mixture}$ is only slightly larger than that predicted for the pure random case, but when 50% of the molecules are clustered, $E_{mixture}$ is substantially increased over E_{random}. The magnitude of the difference between $E_{mixture}$ and E_{random} will depend on the size of *r*, since for a given acceptor surface density, E_{random} becomes smaller as *r* increases (Fig. A2). However, when clusters are present, $E_{clustered}$ dominates $E_{mixture}$ at low acceptor surface densities, where the contribution from the randomly distributed molecules is smallest. Thus, in this case $E_{mixture}$ will not necessarily extrapolate to zero at low surface densities, while E_{random} will. Furthermore since $E_{clustered}$ is a function of D:A (Eqs. A3 and A4), $E_{mixture}$ will also be sensitive to D:A. This is illustrated in Fig. A3 *b*, which shows that for a mixture of randomly distributed monomers and dimers, $E_{mixture}$ increases as a function of increasing mole fraction of acceptor in the D:A mixture (Fig. A3 *b*).

The second limiting case that we will consider for mixed populations occurs when the fraction of clustered versus randomly distributed molecules depends on the surface density of the molecules of interest. To explore this effect, we will use a well-defined model in which acceptors directly bind to randomly distributed donors (Wolber and Hudson, 1979). Although this model is somewhat different from the others that we have discussed (because it assumes that the donors and acceptors are on two different kinds of molecules that form heterodimers), we present it

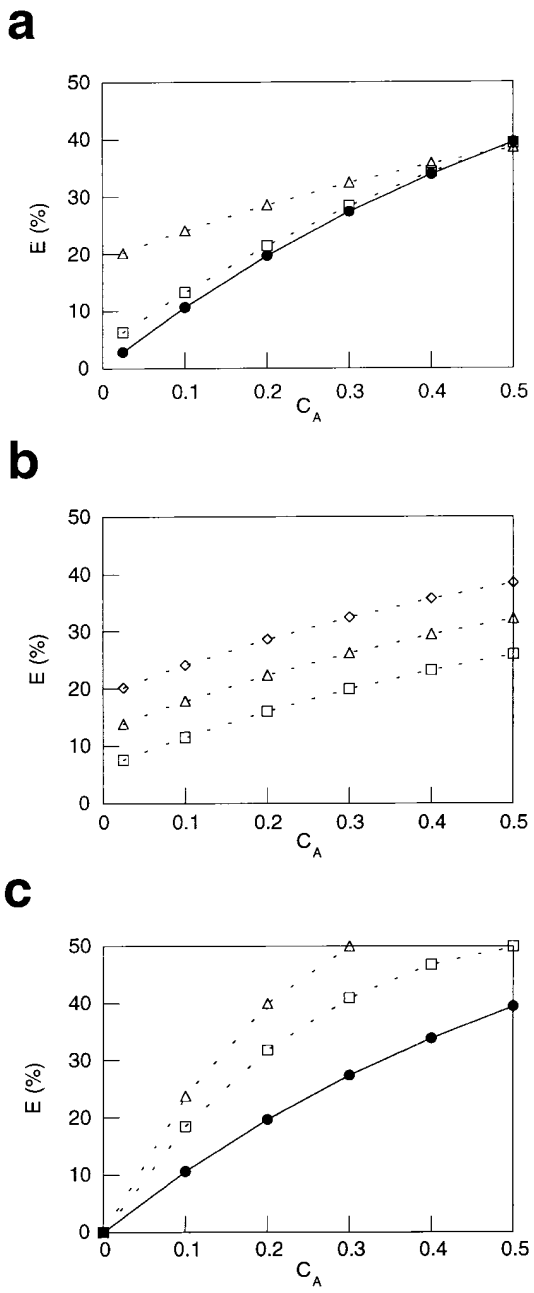

Figure A3. Model calculations for energy transfer efficiency $E_{mixture}$ arising from mixtures of randomly distributed and clustered molecules. The acceptor surface density is represented by the dimensionless parameter c_A. (*a*) Effect of constant mole fraction of clustered molecules ($f_{clustered}$) in the mixture. Model curves were calculated from Eq. A5, setting $r = R_o$, $E_{clustered}$ = 37.5%, and assuming $f_{clustered}$ is either 0.1 (*squares*) or 0.5 (*triangles*). E_{random} for a pure random population was calculated with Eq. A1 assuming $r = R_o$ (*solid circles*). (*b*) Effect of varying D:A. Model curves were calculated from Eq. A5 with $r = R_o$ and $f_{random} = f_{clustered}$ = 0.5. $E_{clustered}$ was calculated using Eq. A4, assuming E_{dimer} = 50%, for D:A = 1:1 (*squares*), 1:2 (*triangles*), or 1:3 (*diamonds*). To match the experimental labeling conditions, the calculations of f_A at the various D:A assume that the concentration of D in the mixture is 25% of the saturating concentration, therefore f_A = 0.25 at D:A = 1:1, 0.5 at 1:2, and 0.75 at 1:3. (*c*) Effect of surface density–dependent clustering, for randomly distributed donors that each can bind one acceptor (to form a heterodimer). Model curves were calculated from Eq. A5 setting $r = R_o$, $E_{clustered}$ = 50%, and $f_{clustered} = c_A / c_D$, assuming c_D = 0.3 (*triangles*) or 0.5 (*squares*). E_{random} for a pure random population was calculated with Eq. A1 assuming $r = R_o$ (*solid circles*).

here because it is a clear example of surface density–dependent clustering. $E_{mixture}$ for this case can be calculated from Eq. A5 by letting f_{random} and E_{random} describe the unbound donors, and $f_{clustered}$ and $E_{clustered}$ describe the acceptor-bound donors. The model assumes that one donor-labeled molecule binds to one acceptor-labeled molecule, such that $f_{clustered} = c_A/c_D$. Thus $f_{clustered}$, f_{random}, and E_{random} are all dependent on the donor surface density, the acceptor surface density, or both. Fig. A3 *c* shows $E_{mixture}$ calculated for several values of donor surface density c_D, setting $E_{clustered} = 50\%$ for a heterodimer. These model calculations show that the contribution of clusters to $E_{mixture}$ is small at low surface densities but becomes increasing large with increasing acceptor surface density (Fig. A3 *c*). This contrasts with the case discussed above (constant $f_{clustered}$) where $E_{mixture}$ is nonzero even in the limit of low surface densities (Fig. A3, *a* and *b*). Finally, since c_D and c_A are proportional to D:A, again in this case $E_{mixture}$ depends on D:A.

Experimental Strategy for Testing the Predictions of the Theoretical Models

The theoretical models presented above predict both quantitative and qualitative differences in *E* for randomly distributed, clustered, and mixed populations. If parameters such as the value of *r* and the geometry of presumed clusters are known, the models could be tested quantitatively by directly comparing the theoretical curves and experimental data. However, even the qualitative differences between these various models should be sufficient to distinguish among them. These differences can be revealed experimentally by asking: (*a*) Is *E* dependent on either donor or acceptor surface density; (*b*) does *E* go to zero at low surface densities; and (*c*) is *E* is sensitive to D:A? The predicted results for each of the distributions are summarized in Table I in the Results section.

We gratefully acknowledge Drs. T. Jovin, D. Arndt-Jovin, and P. Bastiaens (Max-Planck Institute for Biophysical Chemistry, Göttingen, Germany) for introducing us to the imaging FRET method described here. We thank members of the Edidin lab and Dr. A. Hubbard (Johns Hopkins Medical School, Baltimore, MD) and members of her laboratory for their ongoing support and interest in this study. We also thank two anonymous reviewers for a number of suggestions that improved the manuscript. Dr. Y. Ikehara (Fukuoka University School of Medicine, Fukuoka, Japan) and Dr. P. Luzio (University of Cambridge, Cambridge, England) generously provided the rat liver 5′ NT cDNA and the 5′ NT antibodies, respectively. The expert technical assistance of Mr. A. Nechkin, Mrs. T. Wei, and Mr. T. Du with image analysis, flow cytometry, and biotinylation experiments, respectively, is acknowledged. The FRET experiments were performed at the Advanced Microscopy Facility at the Department of Biology at Johns Hopkins University.

This work was supported by 5P01DK44375 from the National Institutes of Health to M. Edidin.

Received for publication 25 August 1997 and in revised form 28 May 1998.

References

Adair, B.D., and D.M. Engelman. 1994. Glycophorin A helical transmembrane domains dimerize in phospholipid bilayers: a resonance energy transfer study. *Biochemistry.* 33:5539–5544.

Adams, S.R., A.T. Harootunian, Y.J. Buechler, S.S. Taylor, and R.Y. Tsien. 1991. Fluorescence ratio imaging of cyclic AMP in single cells. *Nature.* 349:694–697.

Ahmed, S.N., D.A. Brown, and E. London. 1997. On the origin of sphingolipid/cholesterol-rich detergent-insoluble cell membranes: physiological concentrations of cholesterol and sphingolipid induce formation of a detergent-insoluble, liquid-ordered lipid phase in model membranes. *Biochemistry.* 36: 10944–10953.

Airas, L., J. Niemela, M. Salmi, T. Puurunen, D.J. Smith, and S. Jalkanen. 1997. Differential regulation and function of CD73, a glycosyl-phosphatidylinositol-linked 70-kD adhesion molecules, on lymphocytes and endothelial cells. *J. Cell Biol.* 136:421–431.

Arreaza, G., K.A. Melkonian, M. LaFevre-Bernt, and D.A. Brown. 1994. Triton X-100-resistant membrane complexes from cultured kidney epithelial cells contain the Src family protein tyrosine kinase p62yes. *J. Biol. Chem.* 269:19123–19127.

Bacskai, B.J., B. Hochner, M. Mahaut-Smith, S.R. Adams, B.K. Kaang, E.R. Kandel, and R.Y. Tsien. 1993. Spatially resolved dynamics of cAMP and protein kinase A subunits in Aplysia sensory neurons. *Science.* 260:222–226.

Bastiaens, P.I., and T.M. Jovin. 1996. Microspectroscopic imaging tracks the intracellular processing of a signal transduction protein: fluorescent-labeled protein kinase C beta I. *Proc. Natl. Acad. Sci. USA.* 93:8407–8412.

Bastiaens, P.I., I.V. Majoul, P.J. Verveer, H.D. Soling, and T.M. Jovin. 1996. Imaging the intracellular trafficking and state of the AB5 quaternary structure of cholera toxin. *EMBO (Eur. Mol. Biol. Organ.) J.* 15:4246–4253.

Bordier, C. 1981. Phase separation of integral membrane proteins in Triton X-114 solution. *J. Biol. Chem.* 256:1604–1607.

Brewer, C.B. 1994. Cytomegalovirus plasmid vectors for permanent lines of polarized epithelial cells. *Methods Cell Biol.* 43:233–245.

Brown, D.A., and J.K. Rose. 1992. Sorting of GPI-anchored proteins to glycolipid-enriched membrane subdomains during transport to the apical cell surface. *Cell.* 68:533–544.

Brown, D.A., B. Crise, and J.K. Rose. 1989. Mechanism of membrane anchoring affects polarized expression of two proteins in MDCK cells. *Science.* 245: 1499–1501.

Clegg, R.M. 1995. Fluorescence resonance energy transfer. *Curr. Opin. Biotechnol.* 6:103–110.

Clegg, R.M. 1996. Fluorescence resonance energy transfer (FRET). *In* Fluorescence Imaging Spectroscopy and Microscopy. X.F. Wang and B. Herman, editors. John Wiley, New York. 179–252.

Dale, R.E., J. Eisinger, and W.E. Blumberg. 1979. The orientational freedom of molecular probes. The orientation factor in intramolecular energy transfer. *Biophys. J.* 26:161–193.

Dale, R.E., J. Novros, S. Roth, M. Edidin, and L. Brand. 1981. Application of Forster long-range excitation energy transfer to the determination of distributions of fluorescently-labelled concanavalin A-receptor complexes at the surfaces of yeast and of normal and malignant fibroblasts. *In* Fluorescent Probes. G.S. Beddard and M.A. West, editors. Academic Press, New York. 159–181.

Damjanovich, S., G. Vereb, A. Schaper, A. Jenei, J. Matko, J.P. Starink, G.Q. Fox, D.J. Arndt-Jovin, and T.M. Jovin. 1995. Structural hierarchy in the clustering of HLA class I molecules in the plasma membrane of human lymphoblastoid cells. *Proc. Natl. Acad. Sci. USA.* 92:1122–1126.

Dewey, T.G., and M.M. Datta. 1989. Determination of the fractal dimension of membrane protein aggregates using fluorescence energy transfer. *Biophys. J.* 56:415–420.

Dewey, T.G., and G.G. Hammes. 1980. Calculation of fluorescence resonance energy transfer on surfaces. *Biophys. J.* 32:1023–1035.

Edidin, M. 1997. Lipid microdomains in cell surface membranes. *Curr. Opin. Struct. Biol.* 7:528–532.

Field, K.A., D. Holowka, and B. Baird. 1997. Compartmentalized activation of the high affinity immunoglobulin E receptor within membrane domains. *J. Biol. Chem.* 272:4276–4280.

Fra, A.M., E. Williamson, K. Simons, and R.G. Parton. 1994. Detergent-insoluble glycolipid microdomains in lymphocytes in the absence of caveolae. *J. Biol. Chem.* 269:30745–30748.

Fujimoto, T. 1996. GPI-anchored proteins, glycosphingolipids, and sphingomyelin are sequestered to caveolae only after crosslinking. *J. Histochem. Cytochem.* 44:929–941.

Fung, B.K., and L. Stryer. 1978. Surface density determination in membranes by fluorescence energy transfer. *Biochemistry.* 17:5241–5248.

Gadella, T.W., Jr., and T.M. Jovin. 1995. Oligomerization of epidermal growth factor receptors on A431 cells studied by time-resolved fluorescence imaging microscopy. A stereochemical model for tyrosine kinase receptor activation. *J. Cell Biol.* 129:1543–1558.

Gorodinsky, A., and D.A. Harris. 1995. Glycolipid-anchored proteins in neuroblastoma cells form detergent-resistant complexes without caveolin. *J. Cell Biol.* 129:619–627.

Hannan, L.A., and M. Edidin. 1996. Traffic, polarity, and detergent solubility of a glycosylphosphatidylinositol-anchored protein after LDL-deprivation of MDCK cells. *J. Cell Biol.* 133:1265–1276.

Hannan, L.A., M.P. Lisanti, E. Rodriguez-Boulan, and M. Edidin. 1993. Correctly sorted molecules of a GPI-anchored protein are clustered and immobile when they arrive at the apical surface of MDCK cells. *J. Cell Biol.* 120: 353–358.

Harder, T., and K. Simons. 1997. Caveolae, DIGs, and the dynamics of sphingolipid-cholesterol microdomains. *Curr. Opin. Cell Biol.* 9:534–542.

Herman, B. 1989. Resonance energy transfer microscopy. *Methods Cell Biol.* 30:219–243.

Hille, B. 1992. Ionic Channels of Excitable Membranes. Sinauer Associates Inc., Sunderland, MA. 607 pp.

Holowka, D., and B. Baird. 1983*a*. Structural studies on the membrane-bound immunoglobulin E-receptor complex. 1. Characterization of large plasma membrane vesicles from rat basophilic leukemia cells and insertion of amphipathic fluorescent probes. *Biochemistry.* 22:3466–3474.

Holowka, D., and B. Baird. 1983*b*. Structural studies on the membrane-bound immunoglobulin E-receptor complex. 2. Mapping of distances between sites on IgE and membrane surface. *Biochemistry.* 22:3475–3484.

Howell, K.E., U. Reuter-Carlso, E. Devaney, J.P. Luzio, and S.D. Fuller. 1987. One antigen, one gold? A quantitative analysis of immunogold labeling of plasma membrane 5′-nucleotidase in frozen thin sections. *Eur. J. Cell Biol.* 44:318–327.

John, E., and F. Jähnig. 1991. Aggregation state of melittin in lipid vesicle membranes. *Biophys. J.* 60:319–328.

Jovin, T.M., and D.J. Arndt-Jovin. 1989*a*. FRET microscopy: digital imaging of fluorescence resonance energy transfer. Application in cell biology. *In* Cell Structure and Function by Microspectrofluorimetry. E. Kohen, J.S. Ploem, and J.G. Hirschberg, editors. Academic Press, Orlando, FL. 99–117.

Jovin, T.M., and D.J. Arndt-Jovin. 1989*b*. Luminescence digital imaging microscopy. *Annu. Rev. Biophys. Biophys. Chem.* 18:271–308.

Jurgens, L., D. Arndt-Jovin, I. Pecht, and T.M. Jovin. 1996. Proximity relationships between the type I receptor for Fcε (FcεRI) and the mast cell function-associated antigen (MAFA) studied by donor photobleaching fluorescence resonance energy transfer microscopy. *Eur. J. Immunol.* 26:84–91.

Kam, Z., T. Volberg, and B. Geiger. 1995. Mapping of adherens junction components using microscopic resonance energy transfer imaging. *J. Cell Sci.* 108:1051–1062.

Kenworthy, A.K., and M. Edidin. 1998. Imaging fluorescence resonance energy transfer as a probe of the membrane organization and molecular associations of GPI-anchored proteins. *In* Protein Lipidation Protocols. M.H. Gelb and J. Walker, editors. Humana Press, Inc., Totowa, NJ. In press.

Kindzelskii, A.L., W. Xue, R.F. Todd III, and H.R. Petty. 1994. Imaging the spatial distribution of membrane receptors during neutrophil phagocytosis. *J. Struct. Biol.* 113:191–198.

Kindzelskii, A.L., Z.O. Laska, R.F. Todd III, and H.R. Petty. 1996. Urokinase-type plasminogen activator receptor reversibly dissociates from complement receptor type 3 ($\alpha_M\beta_2$, CD11b/CD18) during neutrophil polarization. *J. Immunol.* 156:297–309.

Kubitscheck, U., M. Kircheis, R. Schweitzer-Stenner, W. Dreybrodt, T.M. Jovin, and I. Pecht. 1991. Fluorescence resonance energy transfer on single living cells. Application to binding of monovalent haptens to cell-bound immunoglobulin E. *Biophys. J.* 60:307–318.

Kubitscheck, U., R. Schweitzer-Stenner, D.J. Arndt-Jovin, T.M. Jovin, and I. Pecht. 1993. Distribution of type I Fcε-receptors on the surface of mast cells probed by fluorescence resonance energy transfer. *Biophys. J.* 64:110–120.

Kurzchalia, T.V., E. Hartmann, and P. Dupree. 1995. Guilt by insolubility: does a protein's detergent insolubility reflect a caveolar location? *Trends Cell Biol.* 5:187–189.

Lisanti, M.P., and E. Rodriguez-Boulan. 1990. Glycophospholipid membrane anchoring provides clues to the mechanism of protein sorting in polarized epithelial cells. *Trends Biochem. Sci.* 15:113–118.

Lisanti, M.P., I.W. Caras, M.A. Davitz, and E. Rodriguez-Boulan. 1989. A glycophospholipid membrane anchor acts as an apical targeting signal in polarized epithelial cells. *J. Cell Biol.* 109:2145–2156.

Lisanti, M.P., P.E. Scherer, Z. Tang, and M. Sargiacomo. 1994. Caveolae, caveolin and caveolin-rich membrane domains: a signalling hypothesis. *Trends Cell Biol.* 4:231–235.

Low, M.G. 1989. The glycosyl-phosphatidylinositol anchor of membrane proteins. *Biochim. Biophys. Acta.* 988:427–454.

Matko, J., and M. Edidin. 1997. Energy transfer methods for detecting molecular clusters on cell surfaces. *Methods Enzymol.* 278:444–462.

Mátyus, L. 1992. Fluorescence resonance energy transfer measurements on cell surfaces. A spectroscopic tool for determining protein interactions. *J. Photochem. Photobiol.* 12:323–337.

Mayor, S., and F.R. Maxfield. 1995. Insolubility and redistribution of GPI-anchored proteins at the cell surface after detergent treatment. *Mol. Biol. Cell.* 6:929–944.

Mayor, S., K.G. Rothberg, and F.R. Maxfield. 1994. Sequestration of GPI-anchored proteins in caveolae triggered by cross-linking. *Science*. 264:1948–1951.

Melkonian, K.A., T. Chu, L.B. Tortorella, and D.A. Brown. 1995. Characterization of proteins in detergent-resistant membrane complexes from Madin-Darby canine kidney epithelial cells. *Biochemistry.* 34:16161–16170.

Mescher, M.F., M.J.L. Jose, and S.P. Balk. 1981. Actin-containing matrix associated with the plasma membrane of murine tumour and lymphoid cells. *Nature.* 289:139–144.

Misumi, Y., S. Ogata, S. Hirose, and Y. Ikehara. 1990. Primary structure of rat liver 5′ nucleotidase deduced from the cDNA. *J. Biol. Chem.* 265:2178–2183.

Mujumdar, R.B., L.A. Ernst, S.R. Mujumdar, C.J. Lewis, and A.S. Waggoner. 1993. Cyanine dye labeling reagents: sulfoindocyanine succinimidyl esters. *Bioconjugate Chem.* 4:105–111.

Oida, T., Y. Sako, and A. Kusumi. 1993. Fluorescence lifetime imaging microscopy (flimscopy). Methodology development and application to studies of endosome fusion in single cells. *Biophys. J.* 64:676–685.

Parton, R.G., B. Joggerst, and K. Simons. 1994. Regulated internalization of caveolae. *J. Cell Biol.* 127:1199–1215.

Resta, R., and L.F. Thompson. 1997. T cell signalling through CD73. *Cell. Signal.* 9:131–139.

Rijnboutt, S., G. Jansen, G. Posthuma, J.B. Hynes, J.H. Schornagel, and G.J. Strous. 1996. Endocytosis of GPI-linked membrane folate receptor-α. *J. Cell Biol.* 132:35–47.

Rothberg, K.G., Y. Ying, J.F. Kolhouse, B.A. Kamen, and R.G.W. Anderson. 1990. The glycophospholipid-linked folate receptor internalizes folate without entering the clathrin-coated pit endocytic pathway. *J. Cell Biol.* 110:637–649.

Sargiacomo, M., M. Sudol, Z. Tang, and M.P. Lisanti. 1993. Signal transducing molecules and glycosyl-phosphatidylinositol-linked proteins form a caveolin-rich insoluble complex in MDCK cells. *J. Cell Biol.* 122:789–807.

Schnitzer, J.E., D.P. McIntosh, A.M. Dvorak, J. Liu, and P. Oh. 1995. Separation of caveolae from associated microdomains of GPI-anchored proteins. *Science.* 269:1435–1439.

Schnitzer, J.E., P. Oh, and D.P. McIntosh. 1996. Role of GTP hydrolysis in fission of caveolae directly from plasma membranes. *Science.s* 274:239–242.

Schroeder, R., E. London, and D. Brown. 1994. Interactions between saturated acyl chains confer detergent resistance on lipids and glycosylphosphatidylinositol (GPI)-anchored proteins: GPI-anchored proteins in liposomes and cells show similar behavior. *Proc. Natl. Acad. Sci. USA.* 91:12130–12134.

Selvin, P.R. 1995. Fluorescence resonance energy transfer. *Methods Enzymol.* 246:300–334.

Shaklai, N., J. Yguerabide, and H.M. Ranney. 1977. Interaction of hemoglobin with red blood cell membranes as shown by a fluorescent chromophore. *Biochemistry.* 16:5585–5592.

Siddle, K., E.M. Bailyes, and J.P. Luzio. 1981. A monoclonal antibody inhibiting rat liver 5′ nucleotidase. *FEBS Lett.* 128:103–107.

Simons, K., and E. Ikonen. 1997. Functional rafts in cell membranes. *Nature.* 387:569–572.

Simons, K., and G. van Meer. 1988. Lipid sorting in epithelial cells. *Biochemistry.* 27:6197–6202.

Simons, K., and A. Wandinger-Ness. 1990. Polarized sorting in epithelia. *Cell.* 62:207–210.

Smart, E.J., Y.S. Ying, C. Mineo, and R.G.W. Anderson. 1995. A detergent-free method for purifying caveolae membrane from tissue culture cells. *Proc. Natl. Acad. Sci. USA.* 92:10104–10108.

Snyder, B., and E. Freire. 1982. Fluorescence energy transfer in two dimensions. A numeric solution for random and nonrandom distributions. *Biophys. J.* 40:137–148.

Southwick, P.L., L.A. Ernst, E.W. Tauriello, S R. Parker, R.B. Mujumdar, S.R. Mujumdar, H.A. Clever, and A.S. Waggoner. 1990. Cyanine dye labeling reagents—carboxymethylindocyanine succinimidyl esters. *Cytometry*. 11: 418–430.

Stefanova, I., V. Horejsi, I.J. Ansotegui, W. Knapp, and H. Stockinger. 1991. GPI-anchored cell-surface molecules complexed to protein tyrosine kinases. *Science.* 254:1016–1019.

Strohmeier, G.R., W.I. Lencer, T.W. Patapoff, L.F. Thompson, S.L. Carlson, S.J. Moe, D.K. Carnes, R.J. Mrsny, and J.L. Madara. 1997. Surface expression, polarization, and functional significance of CD73 in human intestinal epithelia. *J. Clin. Invest.* 99:2588–2601.

Tsien, R.Y., B.J. Bacskai, and S.R. Adams. 1993. FRET for studying intracellular signalling. *Trends Cell Biol.* 3:242–245.

Uster, P.S. 1993. In situ resonance energy transfer microscopy: monitoring membrane fusion in living cells. *Methods Enzymol.* 221:239–246.

Uster, P.S., and R.E. Pagano. 1986. Resonance energy transfer microscopy: observations of membrane-bound fluorescent probes in model membranes and in living cells. *J. Cell Biol.* 103:1221–1234.

Veatch, W., and L. Stryer. 1977. The dimeric nature of the gramicidin A transmembrane channel: conductance and fluorescence energy transfer studies of hybrid channels. *J. Mol. Biol.* 113: 89–102.

Weimbs, T., S.H. Low, S.J. Chapin, and K.E. Mostov. 1997. Apical targeting in polarized epithelial cells—there's more afloat than rafts. *Trends Cell Biol.* 7:393–399.

Weisz, O.A., C.E. Machamer, and A.L. Hubbard. 1992. Rat liver dipeptidylpeptidase IV contains competing apical and basolateral targeting information. *J. Biol. Chem.* 267:22282–22288.

Wolber, P.K., and B.S. Hudson. 1979. An analytic solution to the Förster energy transfer problem in two dimensions. *Biophys. J.* 28:197–210.

Wu, M., J. Fan, W. Gunning, and M. Ratman. 1997. Clustering of GPI-anchored folate receptor independent of both cross-linking and association with caveolin. *J. Membr. Biol.* 159:137–147.

Wu, P., and L. Brand. 1994. Resonance energy transfer: methods and applications. *Anal. Biochem.* 218:1–13.

Xue, W., A.L. Kindzelskii, R.F. Todd III, and H.R. Petty. 1994. Physical association of complement receptor type 3 and urokinase-type plasminogen activator receptor in neutrophil membranes. *J. Immunol.* 152:4630–4640.

Yguerabide, J. 1994. Theory for establishing proximity relations in biological membranes by excitation energy transfer measurements. *Biophys. J.* 66:683–693.

Zimet, D.B., B.J. Thevenin, A.S. Verkman, S.B. Shohet, and J.R. Abney. 1995. Calculation of resonance energy transfer in crowded biological membranes. *Biophys. J.* 68:1592–1603.

Zimmermann, H. 1992. 5′ nucleotidase: molecular structure and functional aspects. *Biochem. J.* 285:345–365.